catalysts

MDPI

*Review*

# Titanium Dioxide as the Most Used Photocatalyst for Water Purification: An Overview

**Sanja J. Armaković [1,2,*], Maria M. Savanović [1,2] and Stevan Armaković [2,3]**

[1] University of Novi Sad, Faculty of Sciences, Department of Chemistry, Biochemistry and Environmental Protection, 21000 Novi Sad, Serbia
[2] Association for the International Development of Academic and Scientific Collaboration (AIDASCO), 21000 Novi Sad, Serbia
[3] University of Novi Sad, Faculty of Sciences, Department of Physics, 21000 Novi Sad, Serbia
* Correspondence: sanja.armakovic@dh.uns.ac.rs; Tel.: +381-21-485-2754

**Abstract:** Titanium dioxide ($TiO_2$), one of the most frequently used materials in general, has emerged as an excellent photocatalytic material for environmental applications. In this review, principles and mechanisms of the photocatalytic activity of $TiO_2$ have been analyzed. Structural and physical specificities of $TiO_2$ nanoparticles, such as morphology, crystal structure, and electronic and optical properties, have been considered in the context of photocatalytic applications. A review of the influence of several factors, such as the type and dimensions of photocatalyst particles, pH of the solution, the influence of oxidants/electron acceptors, and light intensity on photocatalytic properties of $TiO_2$, has been provided. Superhydrophilicity as an intrinsic property of the $TiO_2$ surface was discussed through surface reconstruction on $TiO_2$ during the reversible hydrophilic changes. Additionally, attention was paid to improving the photocatalytic properties of $TiO_2$ particles through aggregation and agglomeration.

**Keywords:** $TiO_2$ nanoparticles; photocatalytic degradation processes; physical properties; operational parameters; superhydrophilicity; aggregation and agglomeration



**Citation:** Armaković, S.J.; Savanović, M.M.; Armaković, S. Titanium Dioxide as the Most Used Photocatalyst for Water Purification: An Overview. *Catalysts* **2023**, *13*, 26. https://doi.org/10.3390/catal13010026

Academic Editors: Giuseppina Iervolino, Hideyuki Katsumata, Jose Luis Vilas Vilela, Leire Ruiz-Rubio and Huiyao Wang

Received: 30 November 2022
Revised: 14 December 2022
Accepted: 21 December 2022
Published: 24 December 2022



## 1. Introduction

As soon as it was determined that semiconductors could be efficiently used for obtaining products such as $H_2$ and $O_2$, they were also recognized as efficient photocatalysts for degrading toxic materials. Titanium dioxide ($TiO_2$) is the most prominent photocatalyst [1–3], widely employed due to its great photocatalytic activity, chemical and biological stability, insolubility in water, acid and base environment, resistivity towards corrosion, nontoxicity, low price, and availability in comparison to oxide, sulfide, and other materials [4–6]. Heterogeneous photocatalytic oxidation of organic compounds in an aqueous solution in the presence of $TiO_2$ as photocatalyst provides the opportunity for efficient treatment of waste, drinking, surface, and ground waters, as well as for obtaining the ultraclean water suitable for the pharmaceutical industry and microelectronics. Many organic substances and their intermediates are completely mineralized [7–9]. Depending on the structure of the parent compound, degradation proceeds to carbon dioxide, water, nitrates, chalcogenides, phosphates, and other inorganic ions [10]. However, besides all the mentioned advantages, $TiO_2$ has certain drawbacks regarding its practical application. Due to the large band gap, a minimal amount of radiation from a close UV area of sunlight, only ca. 3–4%, is employed during the photocatalytic process. Therefore, $TiO_2$ is practically inactive when exposed to sunlight [11]. This reduces the applicability of the sun as the most economical light source. Near the Earth's surface, there are 0.2–0.3 mol photons $m^{-2}$ $h^{-1}$ in the range 300–400 nm with a typical UV flux of 20–30 W $m^{-2}$ [12].

Taking into account the serious influence of organic pollutants on the environment, there is a constant need for the development of materials for the efficient elimination of

toxic substances from drinking water [13,14], ground and surface water [15–18], ocean water, sediment and soil [19,20]. In this regard, oxide nanomaterials such as $TiO_2$ have exhibited great potential for practical applications in many areas. Many advantages of $TiO_2$ over the broad range of other nanomaterials have led to the situation where $TiO_2$ is one of the most frequently employed photocatalytic materials.

In this review, we comprehensively introduced the most important features of $TiO_2$ regarding its photocatalytic properties. It is essential to understand its photocatalytic properties, suitable physical and chemical properties, possible modifications using inexpensive methods, applicability to a wide range of compounds, and commercial availability. Finally, a better understanding of $TiO_2$ photocatalytic properties can contribute to its more frequent practical application for water purification.

## 2. Structural Features and Physical Properties of $TiO_2$ Nanoparticles

Understanding the fundamental properties of semiconductor materials governing their photoelectric performance (such as their crystal structure, lattice parameters, and optical and electronic properties) is essential to optimize their performance for photocatalytic applications. This section introduces the fundamentals underlying the photocatalytic performance of nanostructured $TiO_2$.

### *2.1. Crystal Structures of $TiO_2$*

Morphology and the crystal structure of $TiO_2$ principally determine its photocatalytic activity. Therefore, essential factors for $TiO_2$ photocatalytic activity are crystallite size and the specific surface area [21–23]. $TiO_2$ nanostructures with different shapes and titania-based nanocomposites have attracted much attention in research due to their diverse physicochemical characteristics. The 1D $TiO_2$ nanostructures have gained more attention compared to their 0D and 2D counterparts due to the higher aspect ratio, increased surface area, and efficient electronic charge properties [24]. $TiO_2$ exists in two tetragonal forms (rutile and anatase) and one rhombic form (brookite), Figure 1 [25–28]. Brookite is difficult to obtain in laboratory conditions, while rutile and anatase are easily prepared. As a bulk material, rutile is the stable phase; however, solution-phase preparation methods for $TiO_2$ generally favor the anatase structure. These observations are attributed to two main effects: surface energy and precursor chemistry. It has been found that the surface energy of anatase is lower than those of rutile and brookite [28]. The concept of surface energy accurately explains the observed crossover size of about 30 nm where anatase nanoparticles transform to rutile [29]. Secondly, the crystal structure stability has been explained based on a molecular picture. The precursor chemistry determines the nucleation and growth of the different polymorphs of $TiO_2$, which depends on the reactants used [30,31]. A complicating factor in understanding nanoparticle formation is the multitude of experimental conditions used to synthesize the different $TiO_2$ phases, making it challenging to compare mechanisms [28,32].

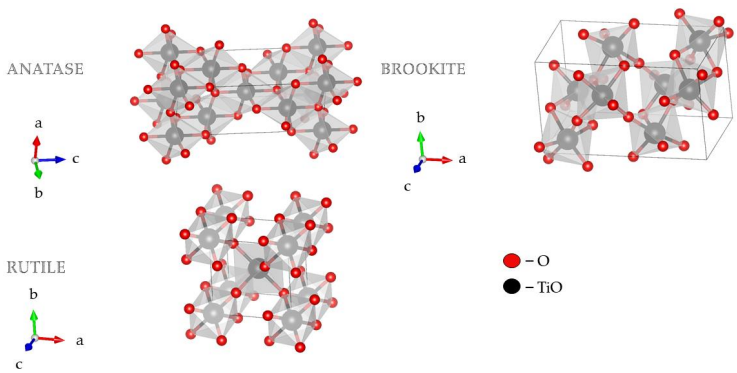


**Figure 1.** 3D visualization crystal structures of $TiO_2$ using visualization for electronic and structural analysis (VESTA) [33].

These polymorphs, anatase, and rutile, exhibit different properties and, consequently, different photocatalytic performances. Of the two tetragonal forms mentioned, the anatase form shows significantly higher photocatalytic activity than rutile due to the higher presence and nature of surface hydroxyl groups. Transformation of anatase form to rutile happens at elevated temperatures of 700–1000 °C. Anatase form is stable at lower temperatures (it occurs in the form of a pyramidal crystal structure). At the same time, rutile (needle-shaped) is dominant during the synthesis at high temperatures [34–36]. Anatase has a higher energy gap, which additionally contributes to the photocatalytic activity of this form. The energy gap of anatase is 3.20 eV, while the rutile energy gap is 3.02 eV [37,38].

$TiO_2$ Degussa P25 is the most frequently used commercial product containing 75% of anatase form and 25% of rutile form [39,40]. The mentioned mixture exhibits outstanding photocatalytic performance and superiority compared with other $TiO_2$ [41]. The predominant form of titania used is anatase. It was found that anatase is the most photocatalytic active form within $TiO_2$ polymorphs. $TiO_2$ Hombikat is a pure anatase form of photocatalyst [39]. $TiO_2$ also appears in another form named $TiO_2$ Wackherr "oxide de titan standard", which contains 100% of anatase form, exhibits interesting characteristics related to photocatalytic application, and is more efficient than $TiO_2$ Degussa P25 [42–44]. The main characteristic of this photocatalyst, when compared with $TiO_2$ Degussa P25, is a lower scattering of radiation in the UV area, which is most likely the consequence of the greater size of particles. Particle size is a crucial factor affecting the performance of nano-photocatalytic materials. The greater size of $TiO_2$ Wackherr particles than $TiO_2$ Degussa P25 results in a lower specific surface area. Particles with a lower specific surface area usually exhibit low photocatalytic activity. However, they can be more efficient in photocatalysis, where optical properties and low scattering are significant [44,45].

### *2.2. Electronic Structure of $TiO_2$*

Understanding the electronic properties of semiconductor materials, including their band structure, nonequilibrium carrier concentration, carrier mobility, and lifetime is essential to achieve inflection of charge carrier behavior and enhancing photocatalytic performance. Against this background, electronic properties of anatase, rutile, and brookite $TiO_2$ phases were introduced [46]. The current understanding of the electronic structures of $TiO_2$ is mainly based on the results of independent and combined theoretical calculations, usually in the framework of the density functional theory (DFT) [26] and experimental techniques (e.g., synchrotron radiation photoelectron spectroscopy, UV-vis spectroscopy, ultraviolet photoelectron spectroscopy, and photoluminescence) [47,48].

The application of various computational methods in elucidating the photocatalytic properties of novel $TiO_2$-based materials is essential. Namely, applying the DFT approach enables researchers to predict the band gap of newly designed materials and focus their attention on synthesizing materials with target photocatalytic properties. The computational aspect of band-gap engineering is critical in developing new photocatalytic materials, as this parameter is essential for practical applications [49]. Additionally, the DFT approach, in combination with carefully selected density functionals and basis sets, is an excellent tool for understanding the light absorption properties of molecules that are degraded by photocatalysts, helping scientists to easier identify the degradation mechanism [50].

Regarding the computational design of novel materials, the DFT approach offers the best cost–efficiency ratio [51]. This flexible theoretical approach allows researchers to elucidate the structural and electronic properties of photocatalytic materials by analyzing how various structural alterations influence the electronic subsystem of nanomaterials.

However, the DFT approach's severe drawback is that it severely underestimates the band gap values due to self-interaction error [52–55]. Considering the fundamental importance of band gaps in photocatalysis, this is a significant challenge in designing novel compounds to be applied in this area. In general, this issue can be tackled in two main ways. One approach is to create specially designed density functionals that reproduce electron density adequately. The second approach is to use the existing density functionals

and implement specific corrections within them. Both directions have positive and negative sides. For example, specially designed hybrid density functionals yield outstanding results in accuracy, but they are computationally much more demanding and are usually applicable only for single-point band structure calculations. Conversely, corrected density functionals offer improved results over conventional density functionals, with computational costs slightly more demanding than traditional density functionals.

Considering the application of hybrid functionals for band structure calculations, it is worth mentioning the importance of the HSE06 hybrid functional [56]. Recent studies have confirmed this function's importance in predicting band gaps of different materials with small, intermediate, and large values of this critical parameter [57,58]. However, in terms of computational costs, hybrid density functionals may still be unavailable to significant number of research groups, which may apply the computationally affordable DFT + U method [59]. This method adds a Hubbard-like term to the Hamiltonian to account for on-site interactions. The simplest version of the DFT + U approach relies on only one parameter—on-site Coulomb term ($U$). However, this method can be improved by incorporating the site exchange term $J$. $U$ and $J$ parameters can be obtained through ab initio applications. Still, they are frequently obtained empirically by testing a range of values. So far, many research studies have reported the values of these parameters for certain types of materials, so a literature survey is warmly recommended to find good starting values.

In Figure 2, we present the band structures and density of states as obtained by applying the DFT + U method, with $U$ taking the value of 7.8 eV and $J$ taking the value of 1 eV, as reported in studies by [60,61]. Inspection of band structures shows that the application of the DFT + U method provides results for band gaps that are in agreement with experimental results, which will be mentioned somewhat later. The density of states figures also show that the conduction band consists of Ti states, while valence band (VB) consists of O states. As reported in reference by Li et al. [62], CB consists of $Ti_{3d}$ states, while VB consists of $O_{2p}$ states.

Ordinarily, $TiO_2$ phases, especially anatase, show good insulation in their ideal stoichiometric states due to their wide bandgap [63]. However, certain types of point defects are unavoidably introduced during the preparation process. These defects might be interstitial titanium ions ($T^{3+}$), oxygen point defects, and substituted ions and can notably affect the charge carrier behavior, band structure, and, eventually, photocatalytic performance [64]. The characteristics of defects (e.g., concentration, type, distribution, and dimension) and their influence on the photoinduced charge carriers in $TiO_2$ can be various [65]. Point defects can induce the generation of defect states, the position generally influenced by the surface and phase. For instance, the defect states of rutile-$TiO_2$ (110) and anatase-$TiO_2$ (101) are found at ≈0.8–1.0 eV and ≈0.4–1.1 eV, of which both are below the CB edge [66]. In the brookite phase, both rutile-like (Y-shaped) and anatase-like (T-shaped) $OTi_3$ building blocks exist, inducing the $O_{2p}$ in VB to present characteristics from both tetragonal phases [26]. Considering the application of hybrid and recently developed density functionals, the study by Dharmale et al. is worth mentioning. In their work, electronic properties such as effective mass, the partial density of states, the total density of states, and the band structure of brookite $TiO_2$ have been studied by applying using seven exchange-correlation functionals, including the already-mentioned HSE06 [67]. Band structures and projected density of states for the rutile), brookite, and anatase polymorphs of $TiO_2$ are shown in Figure 2.

### *2.3. Optical Properties of $TiO_2$*

A semiconductor's optical properties (e.g., photoconductivity, dielectric constant, refractive index, extinction coefficient, reflectivity, absorption coefficient, and loss function) are related to its bandgap [68]. $TiO_2$ is commonly known as a wide-bandgap semiconductor with high susceptibility to UV light [69,70]. The optical absorption in the visible and near-infrared regions is insignificant because photons in the visible region do not have intrinsic excitation of carriers. When the electrons ($e^-$) in the VB are exposed to UV radiation, they

are excited to the CB, leaving holes ($h^+$) in the VB [71–73]. The CB $e^-$ is now in a purely 3D state, and the possibility of transition of $e^-$ to the VB is reduced due to the difference in parity. Therefore, the probability of $e^-$–$h^+$ recombination is reduced [74]. Consequently, separating energy between these two states defines the sensitivity of $TiO_2$ towards the light in the UV range. However, the optical properties at the surface differ considerably from those of the bulk material, providing extensive opportunities to optimize further the photoelectric and optical properties of $TiO_2$ [75].

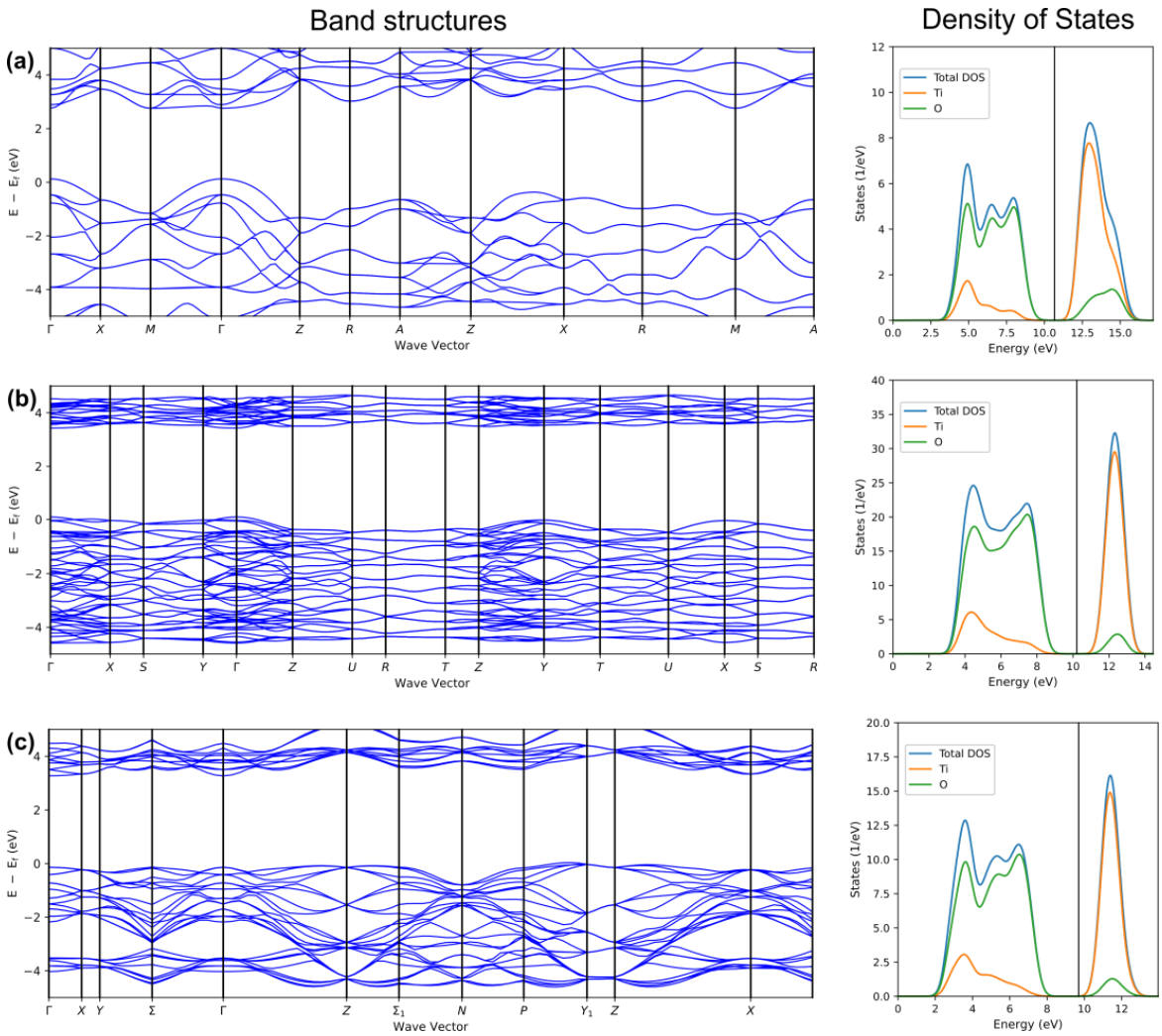


**Figure 2.** Band structures (**left** panel) and projected density of states (**right** panel) for the (**a**) rutile, (**b**) brookite, and (**c**) anatase polymorphs of $TiO_2$, as obtained by DFT + U calculations (PBE functional, GBRV pseudopotentials, $U = 7.8$ eV, $J = 1.0$ eV) in Quantum Espresso program as implemented in Schrödinger Materials Science Suite 2022-4.

The bandgap energies (i.e., optical absorption edges) of rutile, anatase, and brookite $TiO_2$ are estimated to be ≈3.00, 3.21, and 3.13 eV at room temperature, respectively. The photon energy values of optical absorption edges of rutile and anatase increase with the crystal growth temperature decrease [28]. Overall, rutile and anatase bandgaps in bulk are considered to be indirect [76]. Detailed examinations of rutile $TiO_2$ at temperature 1.6 K discover an anisotropic optical response characterized by a direct forbidden transition at ≈3.06 eV. At the same time, the bandgap near the edge is prevailed by an indirect transition. The direct bandgap transition of anatase occurs at ≈3.8–4.0 eV [77]. Additionally, the orthorhombic $TiO_2$ brookite bandgap energy has been experimentally determined to be 3.1–3.4 eV. This is a biaxial material with three independent components other than the

dielectric tensor of the uniaxial rutile and anatase materials [5,28]. The significant value of the energy gap limits the exceptional photocatalytic characteristics of $TiO_2$. Namely, the photon energy should be high enough to excite the $TiO_2$ particles.

In recent experimental and theoretical investigations, efforts have been made to improve the optical properties of $TiO_2$ by increasing its photosensitivity and identifying the correlation between its surface, interfacial, and microstructural characteristics and the corresponding mechanisms crucial to its photoelectric properties [78,79]. Generally used strategies to enhance the optical properties of $TiO_2$ include element doping [80,81] coupled with other semiconductors to form heterojunctions [82,83], synthesis of nanostructures with particular morphologies [84], surface sensitization to improve optical characteristics using organic dyes, metal nanostructures or metal complexes [85], etc.

The doping technique can be explained as the deliberate addition of impurities into a semiconductor material (Figure 3). To enhance $TiO_2$ catalytic activity under visible light, metal/non-metal-doped $TiO_2$ structures have been extensively studied [86]. Adding metal/non-metal increases oxygen vacancies and reduces the band gap energy, resulting in higher photocatalytic activity [87]. This could be useful in wastewater treatment for the photocatalytic degradation of organic compounds under visible and UV light radiation. Many different metals, such as Pd [88], Pt [89], Au, Ag [90], Ce [91], Sr [92], V [93], etc., have been employed for the preparation of metal-doped $TiO_2$ catalysts.

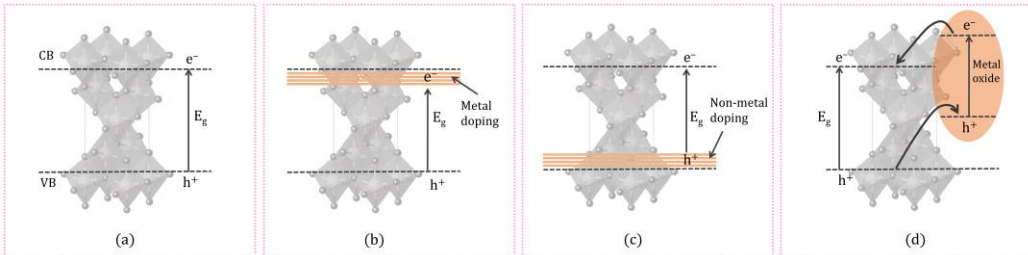


**Figure 3.** Illustrating the generation of photoinduced $e^-$ and $h^+$ in (**a**) pure $TiO_2$, (**b**) metal-doped $TiO_2$, (**c**) non-metal-doped $TiO_2$, and (**d**) coupling $TiO_2$ with the metal oxides.

The sol–gel method is often used in the synthesis, where the photocatalyst is doped with metals such as Fe, Ni, Cr, V, La, Nd, and Sm. The sol–gel process represents one of the versatile methods for preparing nano-dimensional materials. Incorporating an active dopant allows the doped element to interact directly with the support, which is why the material has catalytic or photocatalytic properties. When metal nanoparticles are doped into the $TiO_2$, a new energy level or an interband state is produced in the band gap close to the CB arising from the partially filled d orbitals of the doping metal ions modifying the electronic structure and hence lowering the band gap (Figure 3b).

Although metal-ion doping decreases the energy gap of $TiO_2$, the aforementioned metal ions can also act as recombination centers for electrons and holes, thus reducing the overall activity of the $TiO_2$ [94]. In recent years, non-metals such as C, N, P, S, and B have been the best candidates for obtaining the desired band-gap narrowing of $TiO_2$ [95]. It was shown that non-metal doped $TiO_2$ shows significant catalytic activity under visible light radiation [96]. Several researchers have depicted that $TiO_2$ doping with non-metal ions improve photocatalytic efficiency compared to metals. Doping with cations changes the morphology of the photocatalysts and the photocatalytic activity. It also affects the photocatalyst's electronic structure. Non-metal dopants influence the VB of $TiO_2$ through interactions with 2p $e^-$ of O and form an impurity level above the VB. Distinct non-metals, including N, C, S, F, B, etc., are used as dopants and have shown promising outcomes in recent research studies. Nitrogen doping in $TiO_2$ has gained considerable attention due to its ability to narrow the band gap and promote the electron–hole pair transfer mechanism (Figure 3c). It has been observed that in the case of doping with lighter elements such as N, C, S, or B at substitutional sites of $TiO_2$, lower atomic number elements with smaller

effective nuclear charge appear at a higher localized energy level in the band gap. Doping $TiO_2$ by carbon stabilizes anatase $TiO_2$, enhances its conductivity, and extends the pollutant adsorption on the surface of $TiO_2$ [97].

Žener et al. [87] showed that doping, co-doping, and modifying $TiO_2$ samples with nitrogen, sulfur, and platinum increased their photocatalytic activity by up to 6 times. XRD measurements revealed that the replacement of HCl with $H_2SO_4$ during sol–gel synthesis reduced the size of the crystallites from ~30 nm to ~20 nm, increasing the surface area. This is consistent with the samples' photocatalytic activity and the photocatalysts' measured photocurrent behavior [87].

Coupling $TiO_2$ with the metal oxides increases the charge carrier separation and thereby increases the lifetime of the charge carriers [98]. When the coupled catalyst, consisting of $TiO_2$ and a semiconductor, is irradiated, both the $TiO_2$ and the semiconductor will excite electrons from VB to the CB using UV and Visible irradiation. $TiO_2$ and the semiconductor configuration for coupling are crucial for the enhancement activity. The CB of $TiO_2$ should be more favorable than the corresponding band of the semiconductor, and the VB should be more cathodic than that of $TiO_2$. The $e^-$ from the CB of the semiconductor migrates to the CB of $TiO_2$ and increases the concentration of electrons at the $TiO_2$ conduction band. At the same time, the $h^+$ generated at the VB of $TiO_2$ will be transferred to the VB of the semiconductor, increasing the concentration of $h^+$ in the coupled semiconductor/$TiO_2$ (Figure 3d) [99–101]. Couplings of $TiO_2$ with a metal oxide such as ZnO [102], $SiO_2$ [103], $Cu_2O$ [104], $Bi_2O_3$ or $ZnMn_2O_4$ [105], graphene [106], etc. are reported for many photocatalytic applications including organic pollutant degradation, water splitting, pharmaceutical degradation, etc. $TiO_2$–ZnO binary oxide systems containing various molar ratios of $TiO_2$–ZnO were prepared using a sol–gel method. It was reported that the crystalline structure, thermal stability, and porous structure parameters were determined by the molar ratio of $TiO_2$ to ZnO and the calcination process for the most part. $TiO_2$–ZnO showed high photocatalytic activity towards the degradation of C.I. Basic Blue 9, C.I. Basic Red 1, and C.I. Basic Violet 10 dyes [102]. $TiO_2$ nanoparticles synthesised via the acid-catalysed sol–gel method were used to prepare coupled $TiO_2/SiO_2$ mesoporous materials were prepared by deposition of $TiO_2$ nanoparticles. $TiO_2/SiO_2$ showed photocatalytic activity towards the photodegradation of rhodamine 6G in aqueous solution using UV radiation [103]. One of the noticed studies focuses on $TiO_2$ nanocomposite with graphene as photocatalyst, one of the most prominent representatives of carbon nanostructures. Coupling $TiO_2$ with graphene proved to be beneficial, as the higher efficiency in photocatalysis has been observed compared to that of $TiO_2$ alone. Graphene sheets are thought to act as an electron acceptor that enables the separation and transfer of photogenerated electrons during $TiO_2$ excitation, simultaneously reducing recombination of electron–hole pairs [106]. Wang et al. reported one of the first studies where $TiO_2$ (P25)-graphene nanocomposites were used for photocatalytic degradation of methylene blue. Further research has led to the photodegradation of many organic pollutants by these materials [107].

## 3. Photocatalytic Activity of $TiO_2$: Basic Principles and Mechanism

Exciting species are formed by irradiating $TiO_2$ semiconducting particles with a light of energy higher than the energy gap [108–115]. Namely, electron–hole ($e^-$–$h^+$) pairs are formed (reaction (1)), together with holes in VB and electrons in CB, representing the initial phase of the photocatalytic process (Figure 4) [115].

$$TiO_2 \xrightarrow{hv\ (\lambda < 387\ \mathrm{nm})} TiO_2\left(e^- + h^+\right) \quad (1)$$

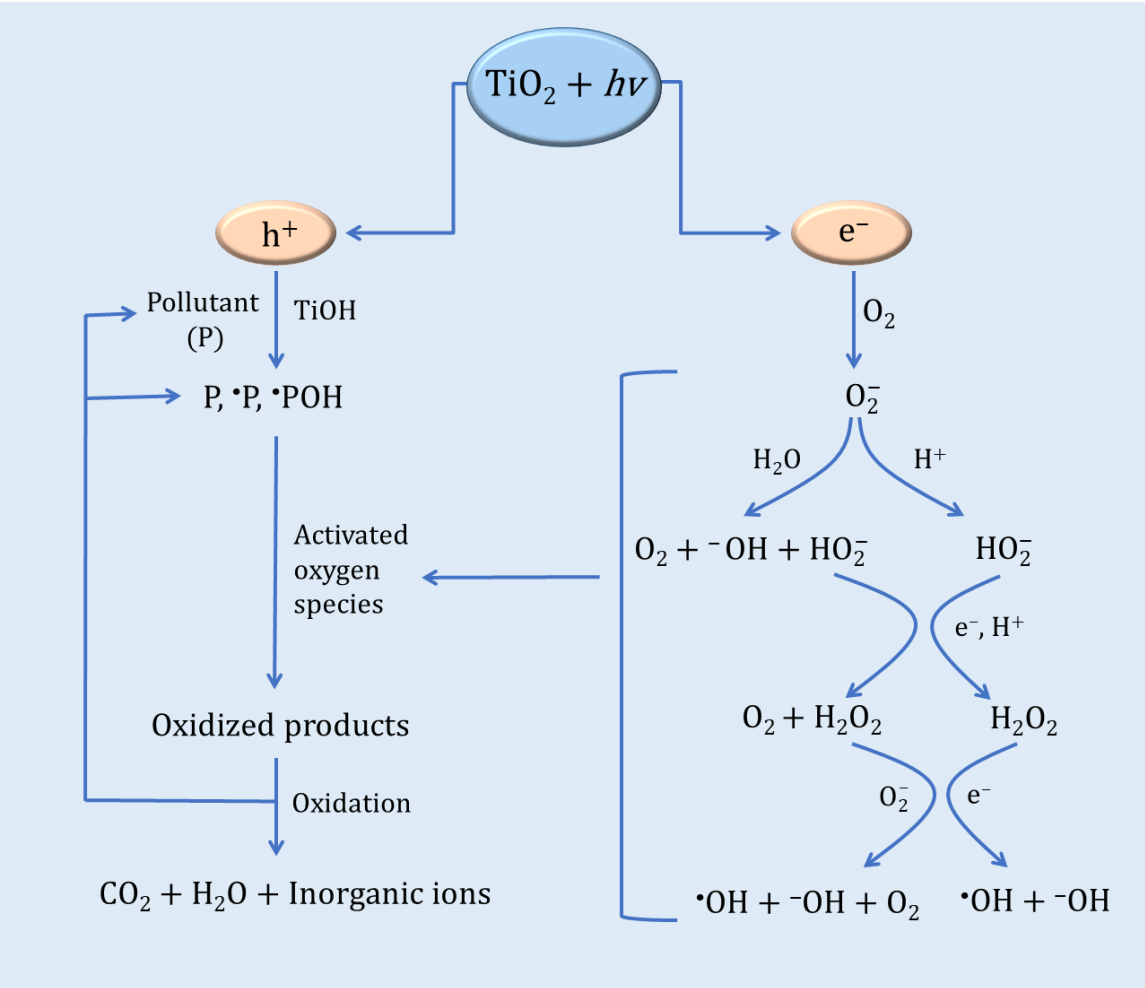


**Figure 4.** Photocatalytic degradation process utilizing $TiO_2$. Adapted with permission from ref. [115] Copyright© 2022 American Chemical Society.

Although the lifetime of $e^-$–$h^+$ pairs is only several nanoseconds, it is enough for a redox reaction with the semiconductor to be initiated [108–110]. Further, formed pairs can be separated or transferred to the surface. Thus, they can take part in the oxide reduction reactions of organic and inorganic compounds, or they can be subjected to the process of recombination (Figure 4), decreasing the quantum yield of the response [108,111]. In an aqueous solution, the surface of $TiO_2$ reacts with $OH^-$ and water molecules which are adsorbed at the surface of the catalyst, by which $^{\bullet}OH$ are formed (reactions (2) and (3)):

$$h^+ + H_2O_{ads} \rightarrow {}^{\bullet}OH_{ads} + H^+ \quad (2)$$

$$h^+ + {}^{-}OH_{ads} \rightarrow {}^{\bullet}OH_{ads} \quad (3)$$

However, one condition has to be achieved for the oxidation of $^-OH$ and water molecules, which are adsorbed on the surface. The redox potential of these reactions has to be lower than the redox potential of the VB of the semiconductor. Reactions (2) and (3) are thermodynamically possible since the aforementioned condition is fulfilled for the $TiO_2$. Since newly formed $^{\bullet}OH$ are powerful oxidizing agents whose standard redox potential is +2.8 V [112–114], they can practically oxidize all organic compounds to mineral products (Figure 4) [115].

Since the redox potentials of many organic compounds are lower than the redox potentials of VB of anatase $TiO_2$, it should be expected for direct oxidation through $h^+$ to occur. However, Turchi and Ollis [116] reported that this does not happen during the pro-

cesses carried in organic solvents, during which complete oxidation of organic compounds does not occur. Other authors believe that direct oxidation of adsorbed reactants, such as carboxyl acids or their anions, employing $h^+$ is possible (reaction (4)) [117,118].

$$h^+ + \text{organic compound} \rightarrow CO_2 + H_2O + \text{inorganic ions} \quad (4)$$

In the case of applying $TiO_2$ as a photocatalyst during processes occurring in an aqueous solution, the share of the reactions through $^{\bullet}OH$ is probably higher (due to the presence of water). However, reactions through $h^+$ could not be neglected [119–121]. In addition to this, applying a fluorescent technique for the quantitative determination of $^{\bullet}OH$ in $TiO_2$ with coumaric and terephthalic acid, it was found that oxidation reactions occur through $h^+$ rather than radicals [122]. Additionally, there are examples where certain authors report that captured $h^+$ and bonded $^{\bullet}OH$ equally participate in the oxidation process [123,124]. $h^+$ transfer to $^{\bullet}OH_{ads}$ after water oxidation on the surface, while $e^-$ from the CB and water molecules are mutual competitors for the takeover of $h^+$. $^{\bullet}OH$ quickly react with the molecules on the catalyst's surface and within the solution and are usually the prominent participants in the photocatalytic reaction [120,125,126].

Phases of the photocatalytic processes are as follows [116,127–129]:

- Excitation of the photocatalyst by photons of energy higher than the energy gap followed by the formation of $e^-$ and $h^+$ (reaction (1));
- Adsorption on the surface of the photocatalyst is followed by reactions (5)–(8):

$$h^+ + P_{ads} \rightarrow TiO_2 + P^+_{ads} \quad (5)$$

$$h^+ + H_2O_{ads} \rightarrow TiO_2 + {}^{\bullet}OH + H^+ \quad (6)$$

$$h^+ + {}^{\bullet}OH_{ads} \rightarrow TiO_2 + {}^{\bullet}OH_{ads} \quad (7)$$

$$e^- + P_{ads} \rightarrow TiO_2 + P^-_{ad} \quad (8)$$

where $P_{ads}$ represent the adsorbed organic molecule;

- "Capturing" of the $e^-$ with $O_2$ as the most commonly used electron acceptor (reaction (9)):

$$e^- + O_2 \rightarrow TiO_2 + O_2^{\bullet -} \quad (9)$$

- Photodegradation by $^{\bullet}OH$, either adsorbed or free, under a variety of free or adsorbed organic species;
- Recombination of the $e^- - h^+$ pairs followed by the heat release (reaction (10)):

$$e^- + h^+ \rightarrow \text{Heat} \quad (10)$$

According to the presented reactions, it can be concluded that the process is rather complex. The extent of the complexity of the process is increased when it is considered that formed radicals can be subjected to the so-called reverse reactions. In such a way, parent compounds can be regenerated [111,130]. The enactment of the reverse reactions influences the photocatalytic process [131]. Therefore, proposing a reaction scheme that considers all formed intermediates is complex. However, the number of researchers finding solutions to these complex mechanisms is increasing, indicating the importance of thie field [120,132,133].

## 4. Factors Affecting Photocatalytic Properties of $TiO_2$

### *4.1. Type and Dimensions of $TiO_2$*

The surface area plays a vital role in the photocatalytic performance of the nanosized porous $TiO_2$. Namely, the higher the surface area, the better the photocatalytic performance of $TiO_2$ will be [134,135]. Different methods can be applied to synthesize $TiO_2$,

influencing the pore structure and crystallite size distribution. Crucial steps of the synthesis procedure can be adjusted to obtain a larger surface area which can offer more active adsorption sites and centers of photocatalytic reaction [136]. Improved photocatalytic activity of mesoporous $TiO_2$ catalysts, in comparison with the microporous materials with restricted pore size, has been reported by several researchers [137–139]. Diffusion of the organic molecules to the active sites on the material surface and optimal exposition to the solar light is achieved through mesoporous $TiO_2$ [138,140]. Since the anatase phase has a much higher photocatalytic activity than amorphous and rutile $TiO_2$, it is still challenging to synthesize mesoporous $TiO_2$ containing the anatase phase of high crystallinity and a large surface area [141,142]. The anatase phase is formed during the calcination process at a temperature of 350 °C and higher [143,144], while the rutile phase is formed as the calcination temperature reaches >600 °C [35,120]. However, high calcination temperature results in nanocrystalline particles' growth and the rapid decrease in the specific surface area [145]. Sol–gel synthesis of nanostructured materials was also intensively explored in the last decade [146–148]. There are many advantages of this approach; some are concerned with the fact that ambient temperature and atmospheric pressure are employed, together with the fact that this process occurs in a solution, offering the control of purity, homogeneity, doping, composition, and stoichiometry. Due to its simplicity and the possibility of controlling structural and morphological properties, sol–gel synthesis is now widely used [149,150]. For nano-dimension particles, recombining photogenerated $e^-$–$h^+$ is much slower than the diffusion of free charge carriers from the particle's interior to its surface, which contributes to the higher photocatalytic activity [151,152]. For the degradation of large organic molecules such as metoprolol [153,154], methylene blue [137,155], paracetamol [156], 3-amino-2-chloropyridine [157], pindolol [158], clopyralid [159], picloram [160], ethylene [161], 4-chlorophenol and methylene orange [162], etc., it was determined that mesoporous $TiO_2$ exhibits high photocatalytic activity. Additionally, photodegradation of stearic acid was achieved using mesoporous and microporous $TiO_2$ films [163], $TiO_2$ self-cleaning films [164], and $TiO_2$ films prepared by template-assisted sol–gel [165]. Mills et al. [166] reported the findings of a detailed study of the photocatalytic properties of Pilkington ActivTM glass in the degradation of stearic acid. Pilkington Glass Activ$^{TM}$ represents a possible successor to Degussa P25 $TiO_2$. Especially as a photocatalyst film for comparing other photocatalysts or superhydrophilitic self-cleaning films. Pilkington Glass Activ$^{TM}$ has superior mechanical stability, reproducible activity, and widespread commercial availability, making it highly attractive as a reference photocatalytic film [166].

Photodegradation of some dyes was very effective in the presence of $TiO_2$. For example, methylene blue was photodegraded using various $TiO_2$ films [167], $TiO_2$ impregnated diatomite [168], $TiO_2$ pretreated with varying concentrations of NaOH [169] brookite–rutile bi-crystalline phase of $TiO_2$ [170], etc. Another dye that has attracted attention due to its frequent decomposition with $TiO_2$ is methyl orange. It was reported that methyl orange was photodegraded using Ag-doped $TiO_2$ photocatalysts [171], carbon nanotubes-$TiO_2$ [172], $TiO_2$-zeolite photocatalyst [173], etc., under visible light and UV irradiation.

These results indicate that it is possible to design photocatalysts possessing molecular size sensitivity. Comparing the properties of $TiO_2$ Wackherr and Degussa P25, $TiO_2$ Wackherr has a much lower specific surface area than Degussa P25 (almost six times). This is the consequence of the much larger particles of Wackherr compared to Degussa P25 [44]. On the other side, Degussa P25 has higher radiation scattering than Wackherr, due to which Degussa P25 is less efficient regarding radiation usage [44,111]. Back reactions often decrease the efficiency of the photocatalytic degradation rates; these reduce partially oxidized transients to give back the initial substrate [44,111,174].

It is well known that photocatalytic activity occurs at the surface of photocatalysts. Therefore, smaller $TiO_2$ nanoparticles, which possess a much higher surface-to-volume ratio, have a greater specific surface area available for catalysis. $TiO_2$ catalysts have been prepared in various nano forms, such as nanoparticle powders, nanotubes, nanorods, nanowires, and immobilized states (as thin films) [86]. Between extensive applications

using surface chemical and physical properties of $TiO_2$, the defects, and the $TiO_2$ surface states, depending enormously on material preparation technologies, play an essential role in its optical, chemical, and electrical properties. Having that in mind, choosing a reliable and well-controllable technology to design the defects in $TiO_2$ is crucial for their specific application [175]. For the preparation of $TiO_2$ thin films, all viable physical and chemical deposition technologies have been used. Over others, atomic layer deposition (ALD) has different advantages due to its precise thickness control, low growth temperature, large area uniformity, and extremely conformal surface coating for nanostructures [176]. Although many precursors have been used successfully for deposition of $TiO_2$ by ALD processes, the common precursor $TiCl_4$, stands out as a liquid with a moderate vapor pressure [177,178]. Active research needs to be continued in the field of $TiO_2$ thin films. This would lead to understanding the synthesis routes, photocatalytic characterization, film morphology, and developing techniques that produce $TiO_2$ thin films with desirable photocatalytic properties while minimizing costs [86].

$TiO_2$ immobilization can be performed on powder and pellet substrates, thick/rigid substrates, or thin/soft materials [179,180]. Titanium oxide-based photocatalytic films can be produced by fused deposition modelling (FDM) by applying biopolymers obtained from renewable biomass resources. This thermoplastic route allows shaping composites through the immobilization of photoactive $TiO_2$ nanoparticles using environmentally friendly bioplastics such as polylactic acid (PLA). Composites synthesized by FDM with an inorganic charge of 30 wt% of $TiO_2$ exhibited a 100% methyl orange (MO) photodegradation after 24 h of light exposition. This could be explained by the extremely uniform dispersion of the nanophase within the polymer matrix in the FDM feedstock [180,181].

### *4.2. UV Light Intensity*

Light intensity is another important factor that influences the process of photocatalytic degradation. Among many factors, light intensity determines the extent of light absorption by semiconducting catalysts at a particular wavelength [12,182–185]. Related to the experimental setup, overall pollutant conversion and degradation efficiency are invariably determined by light intensity distribution within the reactor [186]. According to the reported results by Herrmann [187], the degradation rate can be correlated with the radiant flux, $\Phi$, in the following manner: below the value of 25 mW $cm^{-2}$ for $\Phi$, the degradation rate is proportional to $\Phi$, while for the values of above 25 mW $cm^{-2}$ degradation rate is proportional to $\Phi^{1/2}$. The latter case indicates a high flux value, and an increase in degradation rate is proportional to $\Phi^{1/2}$. Recombination is insignificant for low light intensity. Additionally, the time interval in which the pollutant is exposed to a certain intensity of radiation plays an important role in its degradation, because the longer the pollutant is exposed to radiation, the greater efficiency of degradation could be achieved. Effects of light intensity on the solar photocatalytic degradation of Bisphenol A in water and the presence of $TiO_2$ on sunny and cloudy days were investigated by Kaneco et al. [188]. It was determined that degradation efficiency increases rapidly with the light intensity as $\Phi$ reaches 0.35 mW $cm^{-2}$, after which efficiency increases gradually. In the study of Venkatachalam et al. [147], the mineralization efficiency of 4-chlorophenol was compared when lamps of different wavelengths over $TiO_2$ were used, namely 365 and 254 nm. The results indicated that at 365 nm mineralization rate was somewhat higher than at 254 nm.

It is reported in the literature that the curing behavior of unpigmented coatings is dependent on light intensity [189–192]. A faster cure and even more complete polymerization are achieved with increased light intensity. The influence of different light intensities (in the range from 10–70 mW $cm^{-2}$) on a system which consisted of epoxy acrylate and tri-propylene glycol diacrylate was investigated by Doğruyol et al. [193]. With the increase in light intensity up to 50 mW $cm^{-2}$, the conversion rate and overall conversion increased, while it decreased with the further increase in light intensity. The influence of the light intensity on the photo-polymerization of poly(methacrylic acid) hydrogels was studied

by He et al. [191], and the results of the study indicated that as the UV intensity increased from 2 to 24 mW $cm^{-2}$, the final conversion decreased from 99% to 61%.

However, Mills et al. [166] state that for Degussa P25 $TiO_2$ films, it is difficult to estimate how much light is absorbed and lost through reflection and scattering. Accordingly, they recommend that the photocatalyst system's formal quantum efficiency (FQE) be calculated instead. FQE is the ratio of photoreaction rates and incident light intensity. They further state that the FQE is $\leq$quantum yield for any photochemical process.

The dependence of the rate of conversion and final conversion of pigmented and unpigmented UV curable systems on UV light intensity, ranging from 2 to 80 mW $cm^{-2}$, was investigated by Kardar et al. [189]. Related to unpigmented formulation, it was found that for the intensity ranging from 2 to 20 mW $cm^{-2}$, maximum rates were achieved, and final conversion increased, while the increase in light intensity to 40 and then to 80 mW $cm^{-2}$ decreased the rate of conversion. Related to pigmented formulation, the polymerization and ultimate modification rate increased with the increased light intensity up to 40 mW $cm^{-2}$.

Additionally, the influence of different light intensities (in the range from 5–50 mW $cm^{-2}$) on a system that consisted of UV and monomer benzyl acrylate was investigated by Thiher et al. [194]. Various UV, electron-beam, and hybrid processing conditions were presented for the studies. The processing conditions for electron-beam and UV-only systems were chosen such that the impact of oxygen and additives could be observed. Benzyl acrylate was photopolymerized for 30 s at two different effective irradiances, 20 mW $cm^{-2}$ and 50 mW $cm^{-2}$.

### *4.3. Effect of pH*

The effect of the pH value on the photocatalytic properties of $TiO_2$ is rather complex due to several factors: electrostatic interaction between semiconductor surface, solvent molecules, reactants, and radicals formed during the reaction, etc. [195]. Surface-charge properties of the photocatalyst are influenced by pH value, as shown by Zhu et al. [196]. This fact could be explained based on the point of zero charge (PZC). The adsorbent surface is positively charged, attracting anions and repealing cations when the pH is lower than the PZC. Above the PZC the surface is negatively charged, attracting cations and repealing anions. According to [21,197], this can be represented through the following (reactions (11) and (12)):

$$\mathrm{TiOH} + \mathrm{H}^+ \rightleftarrows \mathrm{TiOH}_2^+ \tag{11}$$

$$\mathrm{TiOH} + {}^{\bullet}\mathrm{OH}_{ads} \rightleftarrows \mathrm{TiO}^- + \mathrm{H_2O} \tag{12}$$

The solution's pH value is essential for heterogeneous photocatalytic reactions since it influences the photocatalyst's surface charge and particle aggregates' size. Based on this data and data for the $pK_a$ of the substrate, degradation can be influenced via electrostatic interactions between the substrate and photocatalyst surface. However, electrostatic interactions are not always crucial for the process. When the pH level is equal to 7 and higher, $^{\bullet}$OH are the main reactive species, while for lower pH levels, the main reactive species are positively charged $h^+$ [198–202]. This also represents essential information since it can be determined through which reactive species the process is being performed.

### *4.4. Effect of Temperature*

The characteristics of $TiO_2$ material could potentially be modified by the temperature [203]. This induces modifications in nanoparticle size, crystalline phase composition, state of aggregation, and optical properties. All these aspects are of underlying importance because they affect the photocatalytic properties of the $TiO_2$ surface [204]. $TiO_2$ potential is highly based on its crystalline structure, average particle size, and morphology [205]. The specific surface area, which depends on particle size, is an essential parameter for the improved catalytical activity of $TiO_2$ [206]. Over time, multiple methods have been employed to prepare $TiO_2$ at the nanoscale level, such as hydrothermal, microemulsion, precipitation, and sol–gel [205,207]. The sol–gel method proved a suitable technique for

synthesizing nanosized $TiO_2$ at low temperatures with high photocatalytic activity, high purity, and homogeneity [208]. The sol–gel process modifies a liquid into a solid phase, sol to gel. The final step of the sol–gel process includes the calcination of colloids at different temperatures and time intervals, which causes the particles' agglomeration and results in causing polydispersity [205].

Chen et al. prepared anatase powder at a calcination temperature of 400 °C, possessing a diameter of 10 nm and a specific surface area of 106.9 $m^2/g$. Additionally, they found a rutile phase at calcination temperatures above 600 °C [209]. Tripathi et al. prepared mixed-phase and pure $TiO_2$ by the sol–gel method calcined at a temperature from 400 °C to 700 °C with a particle size between 19 nm to 68 nm [210]. Velardi et al. [211] synthesized $TiO_2$ powders at different calcination temperatures, which influenced the degree of crystallinity, the phase composition, the optical properties, the nanoparticle dimension, and the photocatalytic activity of $TiO_2$ powders produced by sol–gel method. The obtained results have shown that the temperature increase induces a phase transformation from anatase to rutile. Additionally, a temperature increase leads to the rise in the grain size of $TiO_2$ nanoparticles [211].

### *4.5. Influence of Oxidants/Electron Acceptor*

The addition of electron acceptors significantly increases the efficiency of the photocatalytic process [212,213]. Electron acceptors prevent the recombination of $e^-$–$h^+$ by separation of free charge carriers and an influence of $e^-$ [214–216]. VB and CB for $TiO_2$ originate from the 2p orbital of $O_2$ and 3d orbital of Ti. The role of electron acceptor is most frequently reserved for molecular $O_2$, which is quickly oxidized to $O_2^{\bullet-}$ (reaction (13)) and which is usually adsorbed on the $TiO_2$ surface [217,218]. In this way, the recombination of $e^-$–$h^+$ is prevented, while oxygen radicals are collected and can further take part in the degradation of contaminants [219].

Newly formed $O_2^{\bullet-}$ in acid solution gives $H_2O_2$, which can further oxidize organic compounds (reactions (14) and (15)):

$$e^- + O_{2\ ads} \rightarrow O^{\bullet-}_{2\ ads} \tag{13}$$

$$O_2^{\bullet-} + H^+ \rightarrow HO_2^{\bullet} \tag{14}$$

$$2HO_2^{\bullet} \rightarrow H_2O_2 + O_2 \tag{15}$$

In some cases, photocatalytic activity is completely suppressed without $O_2$. Besides $O_2$, other substances could be used as electron acceptors, such as $H_2O_2$, $KBrO_3$, and $(NH_4)_2S_2O_8$ [199,220–223]. $H_2O_2$ has a significant role in this group of electron acceptors since it efficiently suppresses the recombination of $e^- - h^+$ pairs through reduction with $e^-$ from the CB, which separates the charges (reaction (16)) and it represents the source of additional $^{\bullet}OH$ (reactions (16) and (17)) [224]:

$$H_2O_2 + e^- \rightarrow {}^-OH + {}^{\bullet}OH \tag{16}$$

$$H_2O_2 + hv \rightarrow 2^{\bullet}OH \tag{17}$$

Or $H_2O_2$ reacts with $O_2^{\bullet-}$ btained from $O_2$ in reaction (13) (reaction (18)):

$$H_2O_2 + O_2^{\bullet-} \rightarrow {}^{\bullet}OH + {}^-OH + O_2 \tag{18}$$

where $O_2$ forms, which can further provide and in such a way initiates the process again [199].

$KBrO_3$ and $(NH_4)_2S_2O_8$ through reduction with $e^-$ give radicals which are strong oxidants such as $SO_4^{\bullet-}$ and $BrO_2^{\bullet}$ as in the case of $H_2O_2$. This increases the quantum yield

of processes catalyzed with $TiO_2$. Reactions that include these two radicals are the following (reactions (19)–(22)) [220,225–227]:

$$S_2O_8^{2-} + e^- \rightarrow SO_4^{\bullet -} + SO_4^{2-} \quad (19)$$

$$SO_4^{2-} + H_2O \rightarrow SO_4^{2-} + {}^{\bullet}OH + H^+ \quad (20)$$

$$BrO_3^- + 2H^+ + e^- \rightarrow BrO_2^{\bullet} + H_2O \quad (21)$$

$$BrO_3^- + 6H^+ + 6e^- \rightarrow \left[BrO_2^-, HOBr\right] \rightarrow Br^- + 3H_2O \quad (22)$$

While $e^-$ scavenging and potential involvement of $BrO_2^{\bullet}$ (formed in reaction (21)) could enhance degradation at elevated $BrO_3^-$ levels, the system reactivity could be limited by the formation of $Br^-$ (reaction (22)). The latter could be adsorbed on the photocatalyst surface and involved in $h^+$ and $^{\bullet}OH$ scavenging [66,228,229]. However, although electron acceptors increase the photocatalytic degradation rate, it was found that $H_2O_2$ has an inhibiting effect above the optimal concentrations, i.e., it decreases the degradation rate [199]. Namely, at higher concentrations, a peroxo complex is formed, which interferes with the degradation process, i.e., $H_2O_2$ acts as an absorber of $h^+$ and $^{\bullet}OH$, generating the much less reactive hydroperoxyl/superoxide radicals ($HO_2^{\bullet}/O_2^{\bullet -}$, reaction (23)). Moreover, $HO_2^{\bullet}$ can further react with $^{\bullet}OH$ to form $O_2$ and $H_2O$, which are not directly involved in degradation of organic compound (reaction (24)) [199,228,230,231].

$$H_2O_2 + {}^{\bullet}OH \rightarrow HO_2^{\bullet} + H_2O \left(\text{or } O_2^{\bullet -} + H^+ + H_2O\right) \quad (23)$$

$$HO_2^{\bullet} + {}^{\bullet}OH \rightarrow O_2 + H_2O \quad (24)$$

For this reason, it is necessary to experimentally determine the optimal concentration of the investigated electron acceptor to bypass the negative effect on the process. Regarding electron acceptors, it can be concluded that their influence depends on the nature of the examined substance and the amount of the applied electron acceptor.

### *4.6. Effect of Inorganic Salts*

The ability of some cations to decrease the photodegradation efficiency is related to the fact that they compete with organic compounds for the active sites on the surface of $TiO_2$ [183]. This results in decreased degradation of targeted compounds since the photocatalyst is deactivated. Some examples of cations producing this effect are $Cu^{2+}$ and $Fe^{3+}$. It is determined that $Ca^{2+}$, $Mg^{2+}$, and $Zn^{2+}$ have a negligible effect on the photodegradation of organic compounds. This occurrence is explained by the fact that mentioned cations are in their highest oxidation state [232].

Inorganic anions such as $HCO_3^-$, $CO_3^{2-}$, $Cl^-$, $NO_3^-$ and $SO_4^{2-}$ can be found in wastewater, and their presence causes colloidal instability, an increase in mass transfer, and a decrease in the surface contact between the target molecule and photocatalyst [233]. Consequently, the presence of the mentioned ions results in decreased degradation of organic compounds. Scavenge of $^{\bullet}OH$ through $CO_3^{2-}$ and $HCO_3^-$ can be represented by the following reactions (25)–(27) [183,234]:

$$CO_3^{2-} + {}^{\bullet}OH \rightarrow CO_3^{\bullet -} + {}^{\bullet}OH \quad (25)$$

$$HCO_3^- + {}^{\bullet}OH \rightarrow CO_3^{\bullet -} + H_2O \quad (26)$$

$$CO_3^{\bullet -} + {}^{\bullet}OH \rightarrow HCO_3^- \quad (27)$$

Further, $Cl^-$ and its $h^+$ and $^{\bullet}OH$ scavenging effect (reactions (28)–(30)) decrease the degradation efficiency [235–237].

$$Cl^- + h^+ \rightarrow Cl^{\bullet} \quad (28)$$

$$Cl^- + {}^{\bullet}OH \rightarrow HOCl^{\bullet -} \quad (29)$$

$$HOCl^{\bullet-} + H^+ \rightarrow Cl^{\bullet} + H_2O \quad (30)$$

Further, active sites of the catalyst surface can also be blocked by the formed chloride radical anions. The chloride radicals generated in reactions (28) and (29) have a lower oxidation potential, namely, +2.47 V, than hydroxyl radicals, which have a redox potential of +2.80 V [238].

Wang et al. [239] reported the effect of $NO_3^-$ and $SO_4^{2-}$ on the photodegradation of reactive Red 2 dye under UV irradiation, indicating increased dye removal. Zhu et al. [240] reported that the presence of $NO_3^-$ accelerated the photocatalytic degradation of an azo dye under visible light radiation. The enhancement of the degradation rate by $NO_3^-$ may be principally attributed to the direct or indirect forms of OH, reactions (31)–(33) [240,241]:

$$NO_3^- + hv \rightarrow NO_2^- + O \quad (31)$$

$$NO_3^- + H_2O + hv \rightarrow NO_2^- + {}^{-}OH + {}^{\bullet}OH \quad (32)$$

$$O + H_2O \rightarrow 2^{\bullet}OH \quad (33)$$

$SO_4^{2-}$ in photocatalytic degradation has two crucial roles. It increases aqueous ionic strength by guiding the molecule to the bulk interface, resulting in improved photocatalytic efficiency [242]. Additionally, the adsorbed $SO_4^{2-}$ reacts with generated VB $h^+$ forming $SO_4^{2-}$. This reaction between $SO_4^{2-}$ and photogenerated $h^+$ on the photocatalyst surface can prevent the $e^-$–$h^+$ recombination, enhancing the photodegradation rate (reactions (34) and (35)):

$$SO_4^{2-} + h^+ \rightarrow SO_4^{\bullet-} \quad (34)$$

$$SO_4^{\bullet-} + H_2O \rightarrow SO_4^{2-} + {}^{\bullet}OH + H \quad (35)$$

$SO_4^{\bullet-}$ is a powerful oxidant with a redox potential of +2.6 V, which can enhance the degradation of an organic compound. The degradation rates also depend on the type of salt used. This effect has been studied by various authors [228,243–245].

### *4.7. Superhydrophilicity of $TiO_2$*

The laboratories of TOTO Inc. were conducting experiments, and by accident, they discovered the superhydrophilicity of $TiO_2$. If a $TiO_2$ film was prepared with a certain percentage of $SiO_2$, it was found to acquire superhydrophilic properties, i.e., a water contact angle of ~0° after UV irradiation [246,247]. Additionally, it was found that photo-induced superhydrophilicity was an intrinsic property of the $TiO_2$ surface [248]. Based on the reconstruction of the surface hydroxyl groups under UV irradiation, the mechanism of this process was proposed [249]. Figure 5 illustrates surface reconstruction on $TiO_2$ during the reversible hydrophilic changes. The holes diffuse to the $TiO_2$ surface, trapped at lattice oxygen atoms, while molecular oxygen captures photoexcited electrons. After that, hole capture weakens the binding energy between oxygen in the lattice and Ti atoms. Additionally, another adsorbed water molecule breaks this bond, forming new hydroxyl groups [250]. In the dark, the hydroxyl groups progressively desorb from the surface in the form of $H_2O_2$ or $H_2O$ and $O_2$. Although it seems similar at first glance, the photo-induced hydrophilic conversion is a different process from the photocatalytic degradation of organic pollutants. Strontium titanate, which has almost the same photocatalytic oxidation strength as $TiO_2$, does not become hydrophilic using UV radiation [251]. However, although $WO_3$ exhibits photo-induced hydrophilic conversion, it does not exhibit photocatalytic activity [252]. One unique feature of $TiO_2$ is that there are two different photo-induced phenomena, i.e., photo-induced superhydrophilic phenomenon and photocatalytic phenomenon [253]. Notwithstanding the fact they are different processes, they can, and in fact must take place simultaneously on the same $TiO_2$ surface. The surface can have more superhydrophilic character and less photocatalytic character, or vice versa, which depends on the composition and the processing [11,254].

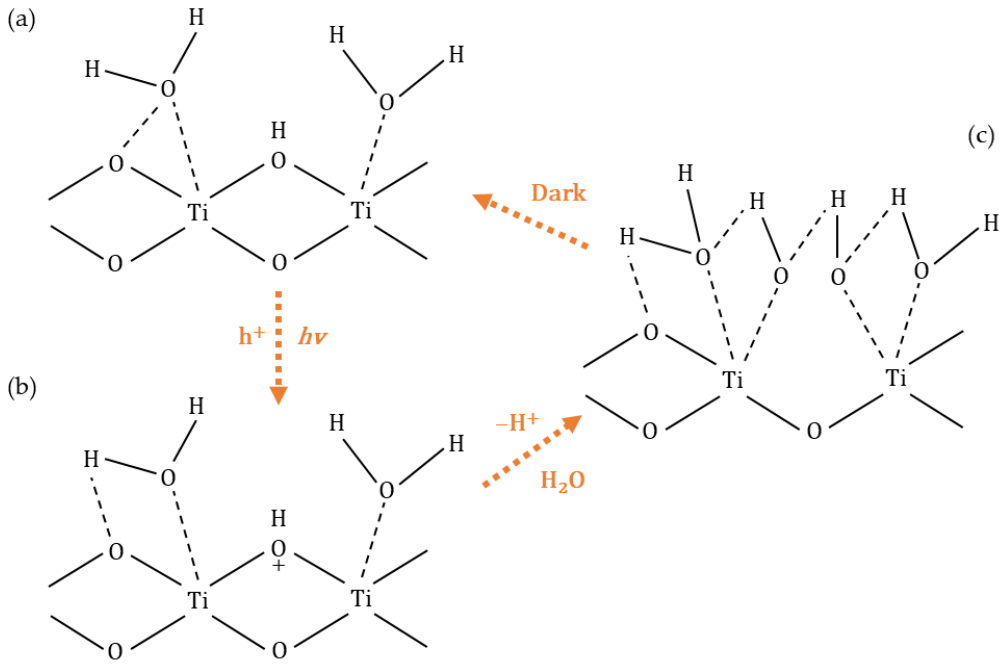


**Figure 5.** Surface reconstruction on $TiO_2$ during the reversible hydrophilic changes: (**a**) before UV irradiation OH group is bound to oxygen vacancy; (**b**) at the transition state, where the photogenerated hole is trapped at the lattice oxygen; and (**c**) after UV irradiation, when new OH groups were formed.

Applications of superhydrophilic technology are widespread nowadays [255]. One example is an antifogging surface which the superhydrophilic effect can prepare. Fogging of glass and mirrors surfaces appears when humid air condenses, with the formation of plenty of tiny water droplets that scatter light. Water droplets can not be formed on a superhydrophilic surface. Instead, a uniform film of water that does not scatter light can be formed on the surface. Additionally, superhydrophilic properties of $TiO_2$ can help the self-cleaning process of $TiO_2$ [255–258].

### *4.8. Aggregation and Agglomeration of $TiO_2$ Particles*

Photocatalyst loading depends strongly on the aggregate particle size when incident radiation is of a wavelength lower than 320 nm. The effect is primarily due to a low penetration depth of the radiation inside the aggregates, limiting the volume fraction of the irradiated aggregates [259].

The fact that three-dimensional $TiO_2$ networks exist in aqueous suspensions served as a solid basis for Wang et al. [260] to propose a novel mechanism for improved photocatalytic processes. From that aspect, it is crucial to understand how the catalyst particles exist in these solutions and, thus, to understand their influence on the catalytic process and its efficiency. If the photocatalytic particles are aggregated/agglomerated and possess the same crystallographic orientation, then the photon energy can be transferred from particle to particle (Figure 6) [259]. This means that even if the targeted molecule is adsorbed on the photocatalytic particle, which is not activated by the photon energy, the photocatalytic process still can take part since the photon energy will be transferred to the particle to which it is adsorbed [71,260–262].

Once the energy has been transferred to the particle "containing" the targeted molecule, the latter will act as a hole trap, and the separation of the original exciton will be induced. So, the basic idea related to the mentioned mechanism is that the agglomeration can be thought of as a long chain of properly aligned $TiO_2$ particles, which allow the transfer of the photon energy from the absorption location to the location of the particle which adsorbed the targeted molecule [263,264].

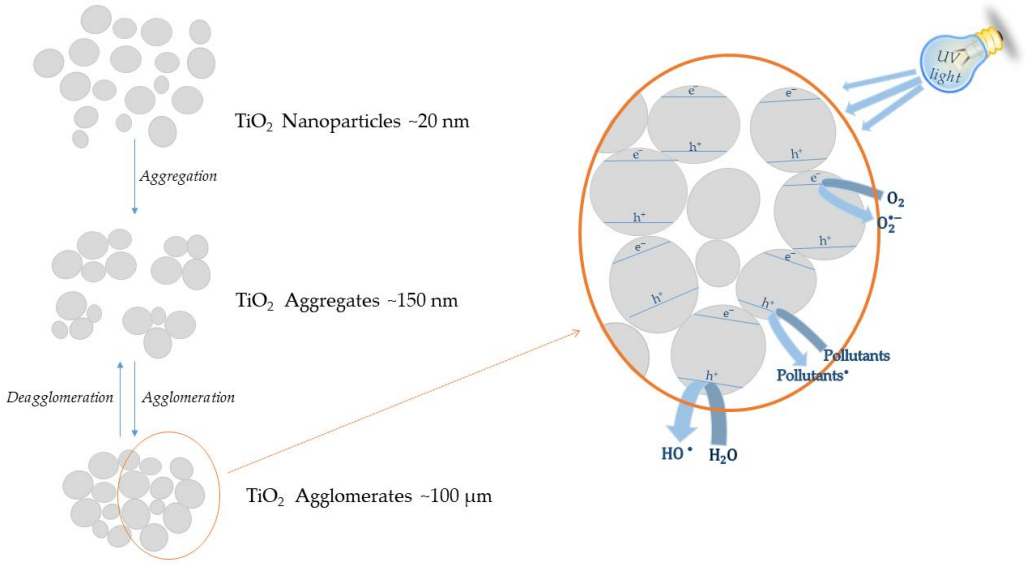


**Figure 6.** Illustration of the aggregation/agglomeration of $TiO_2$ and increased photocatalytic activity through energy transfer.

The aggregation/agglomeration could significantly affect all photocatalytic systems [265,266]. Photocatalytic powders usually consist of nanocrystalline primary particles aggregated to form secondary structures having dimensions in the micrometer range. Improved photocatalytic activity should be achieved when the strong electronic coupling between primary nanoparticles exists [265,267]. As could be concluded, the aggregation and agglomeration could increase the photocatalytic activities of $TiO_2$. Namely, the target molecule does not necessarily need to be located where photon absorption occurs [260,268]. Additionally, the described effect imposes the challenge of designing and synthesizing photocatalytic material with the improved electronic coupling between the semiconducting nanoparticles, which could lead to a breakthrough in the field of photocatalytic degradation [269,270].

## 5. Practical Application

The possibility to activate catalysts with sunlight and recent advances in synthesis methods of the catalyst with desirable band gaps opened the opportunity to design prominent solar collectors where photochemical processes are promoted with the absorption of sunlight. While for solar thermal processes, it is essential to collect as many as possible photons of all wavelengths, for the solar photochemical process, it is crucial to collect only high-energy short-wavelength photons, which are responsible for the initiation of photochemical processes. Usually, for the initiation of solar photochemical processes, UV or near UV sunlight is necessary. However, there are some cases where the sunlight of up to 580 nm can be employed, while 600 nm and higher wavelengths are not usable for these purposes [6]. Initially, photoreactors for photochemical applications were based on line-focus parabolic-trough concentrators. This hardware already existed for solar thermal applications and could be easily modified for photochemical processes. The first European facility for water detoxification based on solar photochemical processes was established in Spain by The Centre for Energy, Environmental and Technological Research. Twelve PTCs were used in this case, while non-concentrating collectors became popular since the influence of concentration and solar tracking does not reduce their efficiency.

Researchers from the Institute of Science and Technology for Ceramics, Italy, developed a $TiO_2$-coated fabric to be used as a photocatalyst agent to degrade Rhodamine B (RhB) in water. They implemented the obtained photocatalytic materials in a 6 L capacity semi-pilot plant. They evaluated the degradation of RhB dye, simulating the water pollution. The good results encouraged the scale-up of the 6 L semi-pilot plant up to the 100 L pilot plant built [271].

Biologically pretreated industrial wastewater from the factories of the Volkswagen AG in Wolfsburg (Germany) and Taubate (Brazil) has been treated in laboratory conditions with great success, after which a pilot plant was installed in the Wolfsburg factory in 1998 [272]. Another project, called "SOLARDETOX", is worth mentioning. The name is an abbreviation for Solar Detoxification Technology for the Treatment of Industrial Non-Biodegradable Persistent Chlorinated Water Contaminants. This project aimed to design and develop a commercial non-concentrating solar detoxification system using neither collecting nor non-collecting collectors but compound parabolic collector technology (CPC), having a concentration ratio equal to 1. CPCs present a particular class of solar collectors produced in the shape of two meeting parabolas. The CPC collector belongs to a non-imaging class of collectors and is considered one of the types with the highest possible concentration ratio. The SOLARDETOX treatment plant is installed at the Hidrocen factory (Madrid, Spain).

Fendrich et al. [273] presented solar concentration technologies for wastewater remediation. They concluded that though mostly on model systems, recent results open promising perspectives for using concentrated sunlight as the energy source powering advanced oxidation processes, such as photocatalytic degradation by $TiO_2$. Additionally, they identified the photocatalyst materials capable of efficiently working with sunlight and the transition to real wastewater investigation as the most critical issues to be addressed by research in the field.

## 6. Conclusions and Outlook

Using clean and self-sustainable technologies is imperative in front of the scientific community. $TiO_2$ belongs to a group of materials with immense practical potential and, by all means, contributes to solving some of the emerging challenges in front of humanity. The energy coming from the Sun is the focus of present and future technologies. In contrast, photocatalysis, a mechanism closely related to this limitless energy source, has been recognized as a rapid and essential strategy to remove environmental pollutants. $TiO_2$ stands out as the best and most commonly used photocatalyst, with a significant advantage over a broad range of nanomaterials.

In this work, we comprehensively introduced the most important features of $TiO_2$ regarding its photocatalytic properties. For the ecological and economical application use of $TiO_2$, it is essential to present the structural characteristics and physical properties of $TiO_2$ nanoparticles. Therefore, this review introduces the fundamentals underlying the photocatalytic performance of nanostructured $TiO_2$ related to its crystal structures and electronic and optical properties. Further, the photocatalytic activity of $TiO_2$ and the mechanism were discussed in detail. Factors that affect photocatalytic properties of $TiO_2$ to the greatest extent, such as type and dimensions of $TiO_2$ particles, UV light intensity, the effect of pH, the influence of oxidants/electron acceptors, and the influence of inorganic salts, were explained. Computational aspects of designing the novel $TiO_2$-based photocatalysis have also been presented. Attention was paid to the superhydrophilicity of $TiO_2$, which is described by two different photo-induced phenomena: photo-induced superhydrophilic and photocatalytic phenomena taking place simultaneously on the same $TiO_2$ surface. Although $TiO_2$ is by far the best nanomaterial, there are still possibilities for its improvement.

**Author Contributions:** Conceptualization, S.J.A. and S.A.; methodology, S.J.A., M.M.S. and S.A.; software, S.J.A. and S.A.; formal analysis, S.J.A., M.M.S. and S.A.; investigation, S.J.A., M.M.S. and S.A.; data curation, S.J.A., M.M.S. and S.A.; writing—original draft preparation, S.J.A., M.M.S. and S.A.; writing—review and editing, S.J.A., M.M.S. and S.A.; visualization, S.J.A. and S.A.; supervision, S.J.A.; project administration, S.J.A. and S.A.; funding acquisition, S.J.A. and S.A. All authors have read and agreed to the published version of the manuscript.

**Funding:** This work is supported by the Ministry of Education, Science and Technological Development of the Republic of Serbia (Grant No. 451-03-68/2022-14/200125).

**Data Availability Statement:** Not applicable.

**Conflicts of Interest:** The authors declare no conflict of interest.

## References


1. Krakowiak, R.; Musial, J.; Bakun, P.; Spychała, M.; Czarczynska-Goslinska, B.; Mlynarczyk, D.T.; Koczorowski, T.; Sobotta, L.; Stanisz, B.; Goslinski, T. Titanium Dioxide-Based Photocatalysts for Degradation of Emerging Contaminants Including Pharmaceutical Pollutants. *Appl. Sci.* **2021**, *11*, 8674. [CrossRef]
2. Elgohary, E.A.; Mohamed, Y.M.A.; El Nazer, H.A.; Baaloudj, O.; Alyami, M.S.S.; El Jery, A.; Assadi, A.A.; Amrane, A. A Review of the Use of Semiconductors as Catalysts in the Photocatalytic Inactivation of Microorganisms. *Catalysts* **2021**, *11*, 1498. [CrossRef]
3. Guerrero, M.; Altube, A.; García-Lecina, E.; Rossinyol, E.; Baró, M.D.; Pellicer, E.; Sort, J. Facile in Situ Synthesis of BiOCl Nanoplates Stacked to Highly Porous $TiO_2$: A Synergistic Combination for Environmental Remediation. *ACS Appl. Mater. Interfaces* **2014**, *6*, 13994–14000. [CrossRef] [PubMed]
4. Lee, S.Y.; Park, S.J. $TiO_2$ Photocatalyst for Water Treatment Applications. *J. Ind. Eng. Chem.* **2013**, *19*, 1761–1769. [CrossRef]
5. Bahadoran, A.; De Lile, J.R.; Masudy-Panah, S.; Sadeghi, B.; Li, J.; Sabzalian, M.H.; Ramakrishna, S.; Liu, Q.; Cavaliere, P.; Gopinathan, A. Photocatalytic Materials Obtained from E-Waste Recycling: Review, Techniques, Critique, and Update. *J. Manuf. Mater. Process.* **2022**, *6*, 69. [CrossRef]
6. Robert, D.; Malato, S. Solar Photocatalysis: A Clean Process for Water Detoxification. *Sci. Total Environ.* **2002**, *291*, 85–97. [CrossRef]
7. Gowland Dan, C.A.; Neil, R.; Efthalia, C. Photocatalytic Oxidation of Natural Organic Matter in Water. *Water* **2020**, *13*, 288. [CrossRef]
8. Uzelac, M.M.; Srđenović Čonić, B.; Kladar, N.; Armaković, S.; Armaković, S.J. Removal of Hydrochlorothiazide from Drinking and Environmental Water: Hydrolysis, Direct and Indirect Photolysis. *Energy Environ.* **2022**, *Article in press*. [CrossRef]
9. Burrows, H.D.; Santaballa, J.A.; Steenken, S. Reaction Pathways and Mechanisms of Photodegradation of Pesticides. *J. Photochem. Photobiol. B Biol.* **2002**, *67*, 71–108. [CrossRef]
10. Menacherry, S.P.M.; Aravind, U.K.; Aravindakumar, C.T. Oxidative Degradation of Pharmaceutical Waste, Theophylline, from Natural Environment. *Atmosphere* **2022**, *13*, 835. [CrossRef]
11. Fujishima, A.; Zhang, X. Titanium Dioxide Photocatalysis: Present Situation and Future Approaches. *Comptes Rendus Chim.* **2006**, *9*, 750–760. [CrossRef]
12. Ahmed, S.; Rasul, M.G.; Martens, W.N.; Brown, R.; Hashib, M.A. Advances in Heterogeneous Photocatalytic Degradation of Phenols and Dyes in Wastewater: A Review. *Water Air Soil Pollut.* **2011**, *215*, 3–29. [CrossRef]
13. Krithiga, T.; Sathish, S.; Renita, A.A.; Prabu, D.; Lokesh, S.; Geetha, R.; Namasivayam, S.K.R.; Sillanpaa, M. Persistent Organic Pollutants in Water Resources: Fate, Occurrence, Characterization and Risk Analysis. *Sci. Total Environ.* **2022**, *831*, 154808.
14. Marathe, D.; Balbudhe, S.; Kumari, K. Persistent Organic Pollutants: A Global Issue, a Global Response. In *Persistent Organic Pollutants*; CRC Press: Boca Raton, FL, USA, 2021; pp. 1–32. ISBN 1003046800.
15. Singh, G.; Singh, A.; Singh, P.; Mishra, V.K. Organic Pollutants in Groundwater Resource. *Groundw. Geochem. Pollut. Remediat. Methods* **2021**, *1*, 139–163.
16. Andreozzi, R.; Caprio, V.; Marotta, R.; Vogna, D. Paracetamol Oxidation from Aqueous Solutions by Means of Ozonation and H2O2/UV System. *Water Res.* **2003**, *37*, 993–1004. [CrossRef]
17. Andreozzi, R.; Caprio, V.; Marotta, R.; Radovnikovic, A. Ozonation and $H_2O_2$/UV Treatment of Clofibric Acid in Water: A Kinetic Investigation. *J. Hazard. Mater.* **2003**, *103*, 233–246. [CrossRef]
18. Sasakova, N.; Gregova, G.; Takacova, D.; Mojzisova, J.; Papajova, I.; Venglovsky, J.; Szaboova, T.; Kovacova, S. Pollution of Surface and Ground Water by Sources Related to Agricultural Activities. *Front. Sustain. Food Syst.* **2018**, *2*, 42. [CrossRef]
19. Ma, Y.; Halsall, C.J.; Crosse, J.D.; Graf, C.; Cai, M.; He, J.; Gao, G.; Jones, K. Persistent Organic Pollutants in Ocean Sediments from the N Orth P Acific to the A Rctic O Cean. *J. Geophys. Res. Ocean.* **2015**, *120*, 2723–2735. [CrossRef]
20. Dachs, J.; Méjanelle, L. Organic Pollutants in Coastal Waters, Sediments, and Biota: A Relevant Driver for Ecosystems during the Anthropocene? *Estuaries Coasts* **2010**, *33*, 1–14. [CrossRef]
21. Behnajady, M.A.; Modirshahla, N. Kinetic Modeling on Photooxidative Degradation of C.I. Acid Orange 7 in a Tubular Continuous-Flow Photoreactor. *Chemosphere* **2006**, *62*, 1543–1548. [CrossRef]
22. Xia, X.H.; Liang, Y.; Wang, Z.; Fan, J.; Luo, Y.S.; Jia, Z.J. Synthesis and Photocatalytic Properties of $TiO_2$ Nanostructures. *Mater. Res. Bull.* **2008**, *43*, 2187–2195. [CrossRef]
23. Ceballos-Chuc, M.C.; Ramos-Castillo, C.M.; Rodríguez-Pérez, M.; Ruiz-Gómez, M.Á.; Rodríguez-Gattorno, G.; Villanueva-Cab, J. Synergistic Correlation in the Colloidal Properties of $TiO_2$ Nanoparticles and Its Impact on the Photocatalytic Activity. *Inorganics* **2022**, *10*, 125. [CrossRef]
24. Reghunath, S.; Pinheiro, D.; KR, S.D. A Review of Hierarchical Nanostructures of $TiO_2$: Advances and Applications. *Appl. Surf. Sci. Adv.* **2021**, *3*, 100063. [CrossRef]
25. Verma, R.; Gangwar, J.; Srivastava, A.K. Multiphase $TiO_2$ Nanostructures: A Review of Efficient Synthesis, Growth Mechanism, Probing Capabilities, and Applications in Bio-Safety and Health. *RSC Adv.* **2017**, *7*, 44199–44224. [CrossRef]
26. Landmann, M.; Rauls, E.; Schmidt, W.G. The Electronic Structure and Optical Response of Rutile, Anatase and Brookite TiO 2. *J. Phys. Condens. Matter* **2012**, *24*, 195503. [CrossRef]

27. Siddiqui, H. Modification of Physical and Chemical Properties of Titanium Dioxide (TiO 2) by Ion Implantation for Dye Sensitized Solar Cells. In *Ion Beam Techniques and Applications*; IntechOpen: London, UK, 2019; ISBN 1789845718.
28. Reyes-Coronado, D.; Rodríguez-Gattorno, G.; Espinosa-Pesqueira, M.E.; Cab, C.; De Coss, R.; Oskam, G. Phase-Pure $TiO_2$ Nanoparticles: Anatase, Brookite and Rutile. *Nanotechnology* **2008**, *19*, 145605. [CrossRef]
29. Navrotsky, A. Energetics of Nanoparticle Oxides: Interplay between Surface Energy and Polymorphism. *Geochem. Trans.* **2003**, *4*, 34. [CrossRef]
30. Li, J.-G.; Ishigaki, T.; Sun, X. Anatase, Brookite, and Rutile Nanocrystals via Redox Reactions under Mild Hydrothermal Conditions: Phase-Selective Synthesis and Physicochemical Properties. *J. Phys. Chem. C* **2007**, *111*, 4969–4976. [CrossRef]
31. Pottier, A.; Chanéac, C.; Tronc, E.; Mazerolles, L.; Jolivet, J.-P. Synthesis of Brookite $TiO_2$ Nanoparticlesby Thermolysis of $TiCl_4$ in Strongly Acidic Aqueous Media. *J. Mater. Chem.* **2001**, *11*, 1116–1121. [CrossRef]
32. Kondamareddy, K.K.; Neena, D.; Lu, D.; Peng, T.; Lopez, M.A.M.; Wang, C.; Yu, Z.; Cheng, N.; Fu, D.J.; Zhao, X.-Z. Ultra-Trace (Parts per Million-Ppm) $W^{6+}$ Dopant Ions Induced Anatase to Rutile Transition (ART) of Phase Pure Anatase $TiO_2$ Nanoparticles for Highly Efficient Visible Light-Active Photocatalytic Degradation of Organic Pollutants. *Appl. Surf. Sci.* **2018**, *456*, 676–693. [CrossRef]
33. Momma, K.; Izumi, F. VESTA 3 for Three-Dimensional Visualization of Crystal, Volumetric and Morphology Data. *J. Appl. Crystallogr.* **2011**, *44*, 1272–1276. [CrossRef]
34. Hanaor, D.A.H.; Sorrell, C.C. Review of the Anatase to Rutile Phase Transformation. *J. Mater. Sci.* **2011**, *46*, 855–874. [CrossRef]
35. Siwińska-Stefańska, K.; Krysztafkiewicz, A.; Ciesielczyk, F.; Paukszta, D.; Sójka-Ledakowicz, J.; Jesionowski, T. Physicochemical and Structural Properties of $TiO_2$ Precipitated in an Emulsion System. *Physicochem. Probl. Miner. Process.* **2010**, *44*, 231–244.
36. Patra, S.; Davoisne, C.; Bouyanfif, H.; Foix, D.; Sauvage, F. Phase Stability Frustration on Ultra-Nanosized Anatase $TiO_2$. *Sci. Rep.* **2015**, *5*, 10928. [CrossRef] [PubMed]
37. Holm, A.; Hamandi, M.; Simonet, F.; Jouguet, B.; Dappozze, F.; Guillard, C. Impact of Rutile and Anatase Phase on the Photocatalytic Decomposition of Lactic Acid. *Appl. Catal. B Environ.* **2019**, *253*, 96–104. [CrossRef]
38. Bhatkhande, D.S.; Pangarkar, V.G.; Beenackers, A.A.C.M. Photocatalytic Degradation for Environmental Applications–a Review. *J. Chem. Technol. Biotechnol. Int. Res. Process. Environ. Clean Technol.* **2002**, *77*, 102–116. [CrossRef]
39. Lan, Y.; Lu, Y.; Ren, Z. Mini Review on Photocatalysis of Titanium Dioxide Nanoparticles and Their Solar Applications. *Nano Energy* **2013**, *2*, 1031–1045. [CrossRef]
40. Lydakis-Simantiris, N.; Riga, D.; Katsivela, E.; Mantzavinos, D.; Xekoukoulotakis, N.P. Disinfection of Spring Water and Secondary Treated Municipal Wastewater by $TiO_2$ Photocatalysis. *Desalination* **2010**, *250*, 351–355. [CrossRef]
41. Chatzitakis, A.; Berberidou, C.; Paspaltsis, I.; Kyriakou, G.; Sklaviadis, T.; Poulios, I. Photocatalytic Degradation and Drug Activity Reduction of Chloramphenicol. *Water Res.* **2008**, *42*, 386–394. [CrossRef]
42. Vijayabalan, A.; Selvam, K.; Krishnakumar, B.; Swaminathan, M. Photocatalytic Degradation of Reactive Orange 4 by Surface Fluorinated $TiO_2$ Wackherr under UV-A Light. *Sep. Purif. Technol.* **2013**, *108*, 51–56. [CrossRef]
43. Selvam, K.; Swaminathan, M. Photocatalytic Synthesis of 2-Methylquinolines with $TiO_2$ Wackherr and Home Prepared $TiO_2$–A Comparative Study. *Arab. J. Chem.* **2017**, *10*, S28–S34. [CrossRef]
44. Vione, D.; Minero, C.; Maurino, V.; Carlotti, M.E.; Picatonotto, T.; Pelizzetti, E. Degradation of Phenol and Benzoic Acid in the Presence of a $TiO_2$-Based Heterogeneous Photocatalyst. *Appl. Catal. B Environ.* **2005**, *58*, 79–88. [CrossRef]
45. Li, D.; Song, H.; Meng, X.; Shen, T.; Sun, J.; Han, W.; Wang, X. Effects of Particle Size on the Structure and Photocatalytic Performance by Alkali-Treated $TiO_2$. *Nanomaterials* **2020**, *10*, 546. [CrossRef]
46. Könenkamp, R. Carrier Transport in Nanoporous TiO 2 Films. *Phys. Rev. B* **2000**, *61*, 11057. [CrossRef]
47. Zhang, K.; Lin, Y.; Muhammad, Z.; Wu, C.; Yang, S.; He, Q.; Zheng, X.; Chen, S.; Ge, B.; Song, L. Active {010} Facet-Exposed $Cu_2MoS_4$ Nanotube as High-Efficiency Photocatalyst. *Nano Res.* **2017**, *10*, 3817–3825. [CrossRef]
48. Che, M.; Védrine, J.C. *Characterization of Solid Materials and Heterogeneous Catalysts: From Structure to Surface Reactivity*; John Wiley & Sons: Hoboken, NJ, USA, 2012; ISBN 3527645330.
49. Kowalska, E.; Wei, Z.; Janczarek, M. Band-Gap Engineering of Photocatalysts: Surface Modification versus Doping. In *Visible-Light-Active Photocatalysis: Nanostructured Catalyst Design, Mechanisms, and Applications*; Wiley: Hoboken, NJ, USA, 2018; pp. 449–484.
50. Armaković, S.; Armaković, S.J. Atomistica. Online–Web Application for Generating Input Files for ORCA Molecular Modelling Package Made with the Anvil Platform. *Mol. Simul.* **2022**, 1–7. [CrossRef]
51. Tsyshevsky, R.V.; Pagoria, P.; Kuklja, M.M. Computational Design of Novel Energetic Materials: Dinitro-Bis-Triazolo-Tetrazine. *J. Phys. Chem. C* **2015**, *119*, 8512–8521. [CrossRef]
52. Perdew, J.P. Density Functional Theory and the Band Gap Problem. *Int. J. Quantum Chem.* **1985**, *28*, 497–523. [CrossRef]
53. Perdew, J.P.; Yang, W.; Burke, K.; Yang, Z.; Gross, E.K.U.; Scheffler, M.; Scuseria, G.E.; Henderson, T.M.; Zhang, I.Y.; Ruzsinszky, A. Understanding Band Gaps of Solids in Generalized Kohn–Sham Theory. *Proc. Natl. Acad. Sci. USA* **2017**, *114*, 2801–2806. [CrossRef]
54. Perdew, J.P.; Levy, M. Physical Content of the Exact Kohn-Sham Orbital Energies: Band Gaps and Derivative Discontinuities. *Phys. Rev. Lett.* **1983**, *51*, 1884. [CrossRef]
55. Mori-Sánchez, P.; Cohen, A.J.; Yang, W. Localization and Delocalization Errors in Density Functional Theory and Implications for Band-Gap Prediction. *Phys. Rev. Lett.* **2008**, *100*, 146401. [CrossRef] [PubMed]

56. Heyd, J.; Scuseria, G.E.; Ernzerhof, M. Hybrid Functionals Based on a Screened Coulomb Potential. *J. Chem. Phys.* **2003**, *118*, 8207–8215. [CrossRef]
57. Borlido, P.; Aull, T.; Huran, A.W.; Tran, F.; Marques, M.A.L.; Botti, S. Large-Scale Benchmark of Exchange–Correlation Functionals for the Determination of Electronic Band Gaps of Solids. *J. Chem. Theory Comput.* **2019**, *15*, 5069–5079. [CrossRef]
58. Borlido, P.; Schmidt, J.; Huran, A.W.; Tran, F.; Marques, M.A.L.; Botti, S. Exchange-Correlation Functionals for Band Gaps of Solids: Benchmark, Reparametrization and Machine Learning. *npj Comput. Mater.* **2020**, *6*, 96. [CrossRef]
59. Cococcioni, M. The LDA+ U Approach: A Simple Hubbard Correction for Correlated Ground States. *Correl. Electrons From Model. Mater. Model. Simul.* **2012**, *2*, 1–33.
60. Zhang, R.; Zhao, J.; Yang, Y.; Lu, Z.; Shi, W. Understanding Electronic and Optical Properties of La and Mn Co-Doped Anatase $TiO_2$. *Comput. Condens. Matter* **2016**, *6*, 5–17. [CrossRef]
61. Chen, W.; Yuan, P.; Zhang, S.; Sun, Q.; Liang, E.; Jia, Y. Electronic Properties of Anatase $TiO_2$ Doped by Lanthanides: A DFT+ U Study. *Phys. B Condens. Matter* **2012**, *407*, 1038–1043. [CrossRef]
62. Li, Z.; Li, Z.; Zuo, C.; Fang, X. Application of Nanostructured $TiO_2$ in UV Photodetectors: A Review. *Adv. Mater.* **2022**, *34*, 2109083. [CrossRef]
63. Yang, H.G.; Sun, C.H.; Qiao, S.Z.; Zou, J.; Liu, G.; Smith, S.C.; Cheng, H.M.; Lu, G.Q. Anatase $TiO_2$ Single Crystals with a Large Percentage of Reactive Facets. *Nature* **2008**, *453*, 638–641. [CrossRef]
64. Zhao, H.; Pan, F.; Li, Y. A Review on the Effects of $TiO_2$ Surface Point Defects on $CO_2$ Photoreduction with $H_2O$. *J. Mater.* **2017**, *3*, 17–32. [CrossRef]
65. Wrana, D.; Gensch, T.; Jany, B.R.; Cieślik, K.; Rodenbücher, C.; Cempura, G.; Kruk, A.; Krok, F. Photoluminescence Imaging of Defects in $TiO_2$: The Influence of Grain Boundaries and Doping on Charge Carrier Dynamics. *Appl. Surf. Sci.* **2021**, *569*, 150909. [CrossRef]
66. Wen, B.; Hao, Q.; Yin, W.-J.; Zhang, L.; Wang, Z.; Wang, T.; Zhou, C.; Selloni, A.; Yang, X.; Liu, L.-M. Electronic Structure and Photoabsorption of Ti 3+ Ions in Reduced Anatase and Rutile TiO 2. *Phys. Chem. Chem. Phys.* **2018**, *20*, 17658–17665. [CrossRef]
67. Dharmale, N.; Chaudhury, S.; Kar, J.K. Various Exchange-Correlation Effects on Structural, Electronic, and Optical Properties of Brookite $TiO_2$. *ECS J. Solid State Sci. Technol.* **2021**, *10*, 83010. [CrossRef]
68. Armaković, S.J.; Mary, Y.S.; Mary, Y.S.; Pelemiš, S.; Armaković, S. Optoelectronic Properties of the Newly Designed 1, 3, 5-Triazine Derivatives with Isatin, Chalcone and Acridone Moieties. *Comput. Theor. Chem.* **2021**, *1197*, 113160. [CrossRef]
69. Del Angel, R.; Durán-Álvarez, J.C.; Zanella, R. $TiO_2$-Low Band Gap Semiconductor Heterostructures for Water Treatment Using Sunlight-Driven Photocatalysis. In *Titanium Dioxide: Material for a Sustainable Environment*; IntechOpen: London, UK, 2018; Volume 305.
70. Etacheri, V.; Di Valentin, C.; Schneider, J.; Bahnemann, D.; Pillai, S.C. Visible-Light Activation of $TiO_2$ Photocatalysts: Advances in Theory and Experiments. *J. Photochem. Photobiol. C Photochem. Rev.* **2015**, *25*, 1–29. [CrossRef]
71. Yang, H.; Yang, B.; Chen, W.; Yang, J. Preparation and Photocatalytic Activities of $TiO_2$ -Based Composite Catalysts. *Catalysts* **2022**, *12*, 1263. [CrossRef]
72. Pawar, M.; Topcu Sendoğdular, S.; Gouma, P. A Brief Overview of $TiO_2$ Photocatalyst for Organic Dye Remediation: Case Study of Reaction Mechanisms Involved in Ce-$TiO_2$ Photocatalysts System. *J. Nanomater.* **2018**, *2018*, 5953609. [CrossRef]
73. Zhang, Z.; Yates, J.T., Jr. Direct Observation of Surface-Mediated Electron− Hole Pair Recombination in $TiO_2$ (110). *J. Phys. Chem. C* **2010**, *114*, 3098–3101. [CrossRef]
74. Kubovics, M.; Silva, G.; Ana, M.L.; Faria, J.L. Photocatalytic Hydrogen Production Using Porous 3D Graphene-Based Aerogels Supporting Pt/$TiO_2$ Nanoparticles. *Gels* **2022**, *8*, 719. [CrossRef]
75. Mosquera-Vargas, E.; Herrera-Molina, D.; Diosa, J.E. Structural and Optical Properties of $TiO_2$ Nanoparticles and Their Photocatalytic Behavior under Visible Light. *Ing. Compet.* **2021**, *23*, 2.
76. Luttrell, T.; Halpegamage, S.; Tao, J.; Kramer, A.; Sutter, E.; Batzill, M. Why Is Anatase a Better Photocatalyst than Rutile?-Model Studies on Epitaxial $TiO_2$ Films. *Sci. Rep.* **2014**, *4*, 4043. [CrossRef] [PubMed]
77. Glassford, K.M.; Chelikowsky, J.R. Optical Properties of Titanium Dioxide in the Rutile Structure. *Phys. Rev. B* **1992**, *45*, 3874. [CrossRef] [PubMed]
78. Govindasamy, G.; Murugasen, P.; Sagadevan, S. Investigations on the Synthesis, Optical and Electrical Properties of $TiO_2$ Thin Films by Chemical Bath Deposition (CBD) Method. *Mater. Res.* **2016**, *19*, 413–419. [CrossRef]
79. Soussi, A.; Ait Hssi, A.; Boujnah, M.; Boulkadat, L.; Abouabassi, K.; Asbayou, A.; Elfanaoui, A.; Markazi, R.; Ihlal, A.; Bouabid, K. Electronic and Optical Properties of $TiO_2$ Thin Films: Combined Experimental and Theoretical Study. *J. Electron. Mater.* **2021**, *50*, 4497–4510. [CrossRef]
80. Huang, F.; Yan, A.; Zhao, H. Influences of Doping on Photocatalytic Properties of $TiO_2$ Photocatalyst. In *Semiconductor Photocatalysis-Materials, Mechanisms and Applications*; InTech: Rang-Du-Fliers, France, 2016; pp. 31–80.
81. Madima, N.; Kefeni, K.K.; Mishra, S.B.; Mishra, A.K.; Kuvarega, A.T. Fabrication of Magnetic Recoverable $Fe_3O_4$/$TiO_2$ Heterostructure for Photocatalytic Degradation of Rhodamine B Dye. *Inorg. Chem. Commun.* **2022**, *145*, 109966. [CrossRef]
82. Amin, S.; Sher, M.; Ali, A.; Rehman, M.F.; Hayat, A.; Ikram, M.; Abbas, A.; Amin, H.M.A. Sulfonamide-Functionalized Silver Nanoparticles as an Analytical Nanoprobe for Selective Ni (II) Sensing with Synergistic Antimicrobial Activity. *Environ. Nanotechnol. Monit. Manag.* **2022**, *18*, 100735. [CrossRef]

83. Kumar, A.; Khan, M.; He, J.; Lo, I.M.C. Recent Developments and Challenges in Practical Application of Visible–Light–Driven $TiO_2$–Based Heterojunctions for PPCP Degradation: A Critical Review. *Water Res.* **2020**, *170*, 115356. [CrossRef]
84. Hua, X.; Liu, Z.; Bruce, P.G.; Grey, C.P. The Morphology of $TiO_2$ (B) Nanoparticles. *J. Am. Chem. Soc.* **2015**, *137*, 13612–13623. [CrossRef]
85. Goulart, S.; Nieves, L.J.J.; Dal Bó, A.G.; Bernardin, A.M. Sensitization of $TiO_2$ Nanoparticles with Natural Dyes Extracts for Photocatalytic Activity under Visible Light. *Dye. Pigment.* **2020**, *182*, 108654. [CrossRef]
86. Varshney, G.; Kanel, S.R.; Kempisty, D.M.; Varshney, V.; Agrawal, A.; Sahle-Demessie, E.; Varma, R.S.; Nadagouda, M.N. Nanoscale $TiO_2$ Films and Their Application in Remediation of Organic Pollutants. *Coord. Chem. Rev.* **2016**, *306*, 43–64. [CrossRef]
87. Žener, B.; Matoh, L.; Reli, M.; Škapin, A.S.; Korošec, R.C. Metal and Non-Metal Modified Titania: The Effect of Phase Composition and Surface Area on Photocatalytic Activity. *Acta Chim. Slov.* **2022**, *69*, 217–226.
88. Wu, J.; Lu, S.; Ge, D.; Zhang, L.; Chen, W.; Gu, H. Photocatalytic Properties of Pd/$TiO_2$ Nanosheets for Hydrogen Evolution from Water Splitting. *RSC Adv.* **2016**, *6*, 67502–67508. [CrossRef]
89. Yu, F.; Wang, C.; Ma, H.; Song, M.; Li, D.; Li, Y.; Li, S.; Zhang, X.; Liu, Y. Revisiting Pt/$TiO_2$ Photocatalysts for Thermally Assisted Photocatalytic Reduction of $CO_2$. *Nanoscale* **2020**, *12*, 7000–7010. [CrossRef]
90. Sadrieyeh, S.; Malekfar, R. Photocatalytic Performance of Plasmonic Au/Ag-$TiO_2$ Aerogel Nanocomposites. *J. Non. Cryst. Solids* **2018**, *489*, 33–39. [CrossRef]
91. Cao, X.; Yang, X.; Li, H.; Huang, W.; Liu, X. Investigation of Ce-$TiO_2$ Photocatalyst and Its Application in Asphalt-Based Specimens for NO Degradation. *Constr. Build. Mater.* **2017**, *148*, 824–832. [CrossRef]
92. Sood, S.; Umar, A.; Mehta, S.K.; Sinha, A.S.K.; Kansal, S.K. Efficient Photocatalytic Degradation of Brilliant Green Using Sr-Doped $TiO_2$ Nanoparticles. *Ceram. Int.* **2015**, *41*, 3533–3540. [CrossRef]
93. Rossi, L.; Palacio, M.; Villabrille, P.I.; Rosso, J.A. V-Doped $TiO_2$ Photocatalysts and Their Application to Pollutant Degradation. *Environ. Sci. Pollut. Res.* **2021**, *28*, 24112–24123. [CrossRef]
94. Zheng, S.K.; Wang, T.M.; Hao, W.C.; Shen, R. Improvement of Photocatalytic Activity of $TiO_2$ Thin Film by Sn Ion Implantation. *Vacuum* **2002**, *65*, 155–159. [CrossRef]
95. Choudhury, B.; Bayan, S.; Choudhury, A.; Chakraborty, P. Narrowing of Band Gap and Effective Charge Carrier Separation in Oxygen Deficient $TiO_2$ Nanotubes with Improved Visible Light Photocatalytic Activity. *J. Colloid Interface Sci.* **2016**, *465*, 1–10. [CrossRef]
96. Yalçın, Y.; Kılıç, M.; Cinar, Z. The Role of Non-Metal Doping in $TiO_2$ Photocatalysis. *J. Adv. Oxid. Technol.* **2010**, *13*, 281–296. [CrossRef]
97. Arora, I.; Chawla, H.; Chandra, A.; Sagadevan, S.; Garg, S. Advances in the Strategies for Enhancing the Photocatalytic Activity of $TiO_2$: Conversion from UV-Light Active to Visible-Light Active Photocatalyst. *Inorg. Chem. Commun.* **2022**, *143*, 109700. [CrossRef]
98. Angela, S.; Lunardi, V.B.; Kusuma, K.; Soetaredjo, F.E.; Putro, J.N.; Santoso, S.P.; Angkawijaya, A.E.; Lie, J.; Gunarto, C.; Kurniawan, A. Facile synthesis of hierarchical porous ZIF-8@$TiO_2$ for simultaneous adsorption and photocatalytic decomposition of crystal violet. *Environ. Nanotechnol. Monit. Manag.* **2021**, *16*, 100598. [CrossRef]
99. Janczarek, M.; Kowalska, E. On the Origin of Enhanced Photocatalytic Activity of Copper-Modified Titania in the Oxidative Reaction Systems. *Catalysts* **2017**, *7*, 317. [CrossRef]
100. Tian, Y.; Yang, H.; Wu, S.; Gong, B.; Xu, C.; Yan, J.; Cen, K.; Bo, Z.; Ostrikov, K. High-performance Water Purification and Desalination by Solar-driven Interfacial Evaporation and Photocatalytic VOC Decomposition Enabled by Hierarchical $TiO_2$-CuO Nanoarchitecture. *Int. J. Energy Res.* **2022**, *46*, 1313–1326. [CrossRef]
101. Humayun, M.; Raziq, F.; Khan, A.; Luo, W. Modification Strategies of $TiO_2$ for Potential Applications in Photocatalysis: A Critical Review. *Green Chem. Lett. Rev.* **2018**, *11*, 86–102. [CrossRef]
102. Siwińska-Stefańska, K.; Kubiak, A.; Piasecki, A.; Goscianska, J.; Nowaczyk, G.; Jurga, S.; Jesionowski, T. $TiO_2$-ZnO Binary Oxide Systems: Comprehensive Characterization and Tests of Photocatalytic Activity. *Materials* **2018**, *11*, 841. [CrossRef]
103. Beyers, E.; Biermans, E.; Ribbens, S.; De Witte, K.; Mertens, M.; Meynen, V.; Bals, S.; Van Tendeloo, G.; Vansant, E.F.; Cool, P. Combined $TiO_2$/SiO2 Mesoporous Photocatalysts with Location and Phase Controllable $TiO_2$ Nanoparticles. *Appl. Catal. B Environ.* **2009**, *88*, 515–524. [CrossRef]
104. Xiong, L.; Yang, F.; Yan, L.; Yan, N.; Yang, X.; Qiu, M.; Yu, Y. Bifunctional Photocatalysis of $TiO_2/Cu_2O$ Composite under Visible Light: $Ti^{3+}$ in Organic Pollutant Degradation and Water Splitting. *J. Phys. Chem. Solids* **2011**, *72*, 1104–1109. [CrossRef]
105. Bessekhouad, Y.; Robert, D.; Weber, J.-V. Photocatalytic Activity of $Cu_2O/TiO_2$, $Bi_2O_3/TiO_2$ and $ZnMn_2O_4/TiO_2$ Heterojunctions. *Catal. Today* **2005**, *101*, 315–321. [CrossRef]
106. Padmanabhan, N.T.; Thomas, N.; Louis, J.; Mathew, D.T.; Ganguly, P.; John, H.; Pillai, S.C. Graphene Coupled $TiO_2$ Photocatalysts for Environmental Applications: A Review. *Chemosphere* **2021**, *271*, 129506. [CrossRef]
107. Wang, W.-S.; Wang, D.-H.; Qu, W.-G.; Lu, L.-Q.; Xu, A.-W. Large Ultrathin Anatase $TiO_2$ Nanosheets with Exposed {001} Facets on Graphene for Enhanced Visible Light Photocatalytic Activity. *J. Phys. Chem. C* **2012**, *116*, 19893–19901. [CrossRef]
108. Chakhtouna, H.; Benzeid, H.; Zari, N.; Bouhfid, R. Recent Progress on Ag/$TiO_2$ Photocatalysts: Photocatalytic and Bactericidal Behaviors. *Environ. Sci. Pollut. Res.* **2021**, *28*, 44638–44666. [CrossRef]
109. Kerketta, U.; Tesler, A.B. Single-Atom Co-Catalysts Employed in Titanium Dioxide Photocatalysis. *Catalysts* **2022**, *12*, 1223. [CrossRef]

110. Bussi, J.; Ohanian, M.; Vázquez, M.; Dalchiele, E.A. Photocatalytic Removal of Hg from Solid Wastes of Chlor-Alkali Plant. *J. Environ. Eng.* **2002**, *128*, 733–739. [CrossRef]
111. Minero, C.; Vione, D. A Quantitative Evalution of the Photocatalytic Performance of $TiO_2$ Slurries. *Appl. Catal. B Environ.* **2006**, *67*, 257–269. [CrossRef]
112. Konstantinou, I.K.; Albanis, T.A. $TiO_2$-Assisted Photocatalytic Degradation of Azo Dyes in Aqueous Solution: Kinetic and Mechanistic Investigations: A Review. *Appl. Catal. B Environ.* **2004**, *49*, 1–14. [CrossRef]
113. Krystynik, P. *Advanced Oxidation Processes (AOPs)–Utilization of Hydroxyl Radical and Singlet Oxygen*; IntechOpen: London, UK, 2021; ISBN 1839682825.
114. Wang, B.; Zhang, H.; Wang, F.; Xiong, X.; Tian, K.; Sun, Y.; Yu, T. Application of Heterogeneous Catalytic Ozonation for Refractory Organics in Wastewater. *Catalysts* **2019**, *9*, 241. [CrossRef]
115. Hoffmann, M.R.; Martin, S.T.; Choi, W.; Bahnemann, D.W. Environmental Applications of Semiconductor Photocatalysis. *Chem. Rev.* **1995**, *95*, 69–96. [CrossRef]
116. Turchi, C.S.; Ollis, D.F. Photocatalytic Degradation of Organic Water Contaminants: Mechanisms Involving Hydroxyl Radical Attack. *J. Catal.* **1990**, *122*, 178–192. [CrossRef]
117. Jiang, D.; Zhao, H.; Zhang, S.; John, R. Kinetic Study of Photocatalytic Oxidation of Adsorbed Carboxylic Acids at $TiO_2$ Porous Films by Photoelectrolysis. *J. Catal.* **2004**, *223*, 212–220. [CrossRef]
118. Herrmann, J.-M.; Guillard, C. Photocatalytic Degradation of Pesticides in Agricultural Used Waters. *Comptes Rendus L'académie Des Sci. IIC Chem.* **2000**, *3*, 417–422. [CrossRef]
119. Santiago-Morales, J.; Agüera, A.; del Gómez, M.M.; Fernández-Alba, A.R.; Giménez, J.; Esplugas, S.; Rosal, R. Transformation Products and Reaction Kinetics in Simulated Solar Light Photocatalytic Degradation of Propranolol Using Ce-Doped $TiO_2$. *Appl. Catal. B Environ.* **2013**, *129*, 13–29. [CrossRef]
120. Yang, H.; Li, G.; An, T.; Gao, Y.; Fu, J. Photocatalytic Degradation Kinetics and Mechanism of Environmental Pharmaceuticals in Aqueous Suspension of $TiO_2$: A Case of Sulfa Drugs. *Catal. Today* **2010**, *153*, 200–207. [CrossRef]
121. Anucha, C.B.; Altin, I.; Bacaksiz, E.; Stathopoulos, V.N. Titanium Dioxide ($TiO_2$)-Based Photocatalyst Materials Activity Enhancement for Contaminants of Emerging Concern (CECs) Degradation: In the Light of Modification Strategies. *Chem. Eng. J. Adv.* **2022**, *10*, 100262. [CrossRef]
122. Ishibashi, K.; Fujishima, A.; Watanabe, T.; Hashimoto, K. Detection of Active Oxidative Species in $TiO_2$ Photocatalysis Using the Fluorescence Technique. *Electrochem. Commun.* **2000**, *2*, 207–210. [CrossRef]
123. Nosaka, Y.; Nosaka, A.Y. Generation and Detection of Reactive Oxygen Species in Photocatalysis. *Chem. Rev.* **2017**, *117*, 11302–11336. [CrossRef]
124. Du, Y.; Rabani, J. The Measure of $TiO_2$ Photocatalytic Efficiency and the Comparison of Different Photocatalytic Titania. *J. Phys. Chem. B* **2003**, *107*, 11970–11978. [CrossRef]
125. Linsebigler, A.L.; Lu, G.; Yates, J.T., Jr. Photocatalysis on $TiO_2$ Surfaces: Principles, Mechanisms, and Selected Results. *Chem. Rev.* **1995**, *95*, 735–758. [CrossRef]
126. Chiu, Y.-H.; Chang, T.-F.M.; Chen, C.-Y.; Sone, M.; Hsu, Y.-J. Mechanistic Insights into Photodegradation of Organic Dyes Using Heterostructure Photocatalysts. *Catalysts* **2019**, *9*, 430. [CrossRef]
127. Alikarami, M.; Soltani, R.D.C.; Khataee, A. An Innovative Combination of Electrochemical and Photocatalytic Processes for Decontamination of Bisphenol A Endocrine Disruptor Form Aquatic Phase: Insight into Mechanism, Enhancers and Bio-Toxicity Assay. *Sep. Purif. Technol.* **2019**, *220*, 42–51. [CrossRef]
128. Kabra, K.; Chaudhary, R.; Sawhney, R.L. Treatment of Hazardous Organic and Inorganic Compounds through Aqueous-Phase Photocatalysis: A Review. *Ind. Eng. Chem. Res.* **2004**, *43*, 7683–7696. [CrossRef]
129. Chong, M.N.; Jin, B.; Chow, C.W.K.; Saint, C. Recent Developments in Photocatalytic Water Treatment Technology: A Review. *Water Res.* **2010**, *44*, 2997–3027. [CrossRef] [PubMed]
130. Liochev, S.I. Reactive Oxygen Species and the Free Radical Theory of Aging. *Free Radic. Biol. Med.* **2013**, *60*, 1–4. [CrossRef] [PubMed]
131. Sharma, S.; Kumar, R.; Raizada, P.; Ahamad, T.; Alshehri, S.M.; Nguyen, V.-H.; Thakur, S.; Nguyen, C.C.; Kim, S.Y.; Van Le, Q. An Overview on Recent Progress in Photocatalytic Air Purification: Metal-Based and Metal-Free Photocatalysis. *Environ. Res.* **2022**, *214*, 113995. [CrossRef] [PubMed]
132. Mehara, J.; Roithová, J. Identifying Reactive Intermediates by Mass Spectrometry. *Chem. Sci.* **2020**, *11*, 11960–11972. [CrossRef]
133. Halasz, A.; Hawari, J.; Perreault, N.N. LC-MS Analysis Data of Intermediate Products Used to Construct Photodegradation Pathways for Bis (1H-Tetrazol-5-Yl) Amine (H2BTA). *Data Br.* **2020**, *28*, 104936. [CrossRef]
134. Gahlot, S.; Dappozze, F.; Mishra, S.; Guillard, C. High Surface Area G-$C_3N_4$ and g-$C_3N_4$-$TiO_2$ Photocatalytic Activity under UV and Visible Light: Impact of Individual Component. *J. Environ. Chem. Eng.* **2021**, *9*, 105587. [CrossRef]
135. Demirors, A.F.; van Blaaderen, A.; Imhof, A. Synthesis of Eccentric Titania− Silica Core− Shell and Composite Particles. *Chem. Mater.* **2009**, *21*, 979–984. [CrossRef]
136. Kim, D.S.; Han, S.J.; Kwak, S.-Y. Synthesis and Photocatalytic Activity of Mesoporous $TiO_2$ with the Surface Area, Crystallite Size, and Pore Size. *J. Colloid Interface Sci.* **2007**, *316*, 85–91. [CrossRef]
137. Kim, E.-Y.; Kim, D.-S.; Ahn, B.-T. Synthesis of Mesoporous $TiO_2$ and Its Application to Photocatalytic Activation of Methylene Blue and E. Coli. *Bull. Korean Chem. Soc.* **2009**, *30*, 193–196.

138. Tan, Y.N.; Wong, C.L.; Mohamed, A.R. An Overview on the Photocatalytic Activity of Nano-Doped-$TiO_2$ In the Degradation of Organic Pollutants. *Int. Sch. Res. Not.* **2011**, *2011*, 261219. [CrossRef]
139. He, K.; Zhao, C.; Zhao, G.; Han, G. Effects of Pore Size on the Photocatalytic Activity of Mesoporous $TiO_2$ Prepared by a Sol–Gel Process. *J. Sol Gel Sci. Technol.* **2015**, *75*, 557–563. [CrossRef]
140. Alagarasi, A.; Rajalakshmi, P.U.; Shanthi, K.; Selvam, P. Solar-Light Driven Photocatalytic Activity of Mesoporous Nanocrystalline $TiO_2$, $SnO_2$, and $TiO_2$-$SnO_2$ Composites. *Mater. Today Sustain.* **2019**, *5*, 100016. [CrossRef]
141. Luo, Z.; Poyraz, A.S.; Kuo, C.-H.; Miao, R.; Meng, Y.; Chen, S.-Y.; Jiang, T.; Wenos, C.; Suib, S.L. Crystalline Mixed Phase (Anatase/Rutile) Mesoporous Titanium Dioxides for Visible Light Photocatalytic Activity. *Chem. Mater.* **2015**, *27*, 6–17. [CrossRef]
142. Yu, J.C.; Zhang, L.; Zheng, Z.; Zhao, J. Synthesis and Characterization of Phosphated Mesoporous Titanium Dioxide with High Photocatalytic Activity. *Chem. Mater.* **2003**, *15*, 2280–2286. [CrossRef]
143. Ferreira, V.R.A.; Azenha, M. Crystallization of Hollow $TiO_2$ into Anatase at Mild Conditions, for Improved Surface Recognition in Selective Photocatalysis. Available online: https://papers.ssrn.com/sol3/papers.cfm?abstract_id=4133307 (accessed on 23 December 2022.).
144. Chang, H.-S.; Choo, K.-H.; Lee, B.; Choi, S.-J. The Methods of Identification, Analysis, and Removal of Endocrine Disrupting Compounds (EDCs) in Water. *J. Hazard. Mater.* **2009**, *172*, 1–12. [CrossRef]
145. Kusuma, M.; Chandrappa, G.T. Effect of Calcination Temperature on Characteristic Properties of $CaMoO_4$ Nanoparticles. *J. Sci. Adv. Mater. Devices* **2019**, *4*, 150–157. [CrossRef]
146. Bokov, D.; Turki Jalil, A.; Chupradit, S.; Suksatan, W.; Javed Ansari, M.; Shewael, I.H.; Valiev, G.H.; Kianfar, E. Nanomaterial by Sol-Gel Method: Synthesis and Application. *Adv. Mater. Sci. Eng.* **2021**, *2021*, 5102014. [CrossRef]
147. Venkatachalam, N.; Palanichamy, M.; Murugesan, V. Sol–Gel Preparation and Characterization of Alkaline Earth Metal Doped Nano $TiO_2$: Efficient Photocatalytic Degradation of 4-Chlorophenol. *J. Mol. Catal. A Chem.* **2007**, *273*, 177–185. [CrossRef]
148. Tajer-Kajinebaf, V.; Sarpoolaky, H.; Mohammadi, T. Sol–Gel Synthesis of Nanostructured Titania–Silica Mesoporous Membranes with Photo-Degradation and Physical Separation Capacities for Water Purification. *Ceram. Int.* **2014**, *40*, 1747–1757. [CrossRef]
149. Navas, D.; Fuentes, S.; Castro-Alvarez, A.; Chavez-Angel, E. Review on Sol-Gel Synthesis of Perovskite and Oxide Nanomaterials. *Gels* **2021**, *7*, 275. [CrossRef] [PubMed]
150. Danks, A.E.; Hall, S.R.; Schnepp, Z. The Evolution of 'Sol–Gel'Chemistry as a Technique for Materials Synthesis. *Mater. Horizons* **2016**, *3*, 91–112. [CrossRef]
151. Colmenares, J.C.; Luque, R.; Campelo, J.M.; Colmenares, F.; Karpiński, Z.; Romero, A.A. Nanostructured Photocatalysts and Their Applications in the Photocatalytic Transformation of Lignocellulosic Biomass: An Overview. *Materials* **2009**, *2*, 2228–2258. [CrossRef]
152. Suhaimi, N.A.A.; Kong, C.P.Y.; Shahri, N.N.M.; Nur, M.; Hobley, J.; Usman, A. Dynamics of Diffusion-and Immobilization-Limited Photocatalytic Degradation of Dyes by Metal Oxide Nanoparticles in Binary or Ternary Solutions. *Catalysts* **2022**, *12*, 1254. [CrossRef]
153. Czech, B.; Rubinowska, K. $TiO_2$-Assisted Photocatalytic Degradation of Diclofenac, Metoprolol, Estrone and Chloramphenicol as Endocrine Disruptors in Water. *Adsorption* **2013**, *19*, 619–630. [CrossRef]
154. De Ceglie, C.; Pal, S.; Murgolo, S.; Licciulli, A.; Mascolo, G. Investigation of Photocatalysis by Mesoporous Titanium Dioxide Supported on Glass Fibers as an Integrated Technology for Water Remediation. *Catalysts* **2022**, *12*, 41. [CrossRef]
155. Ahmed, M.A.; Abou-Gamra, Z.M.; Salem, A.M. Photocatalytic Degradation of Methylene Blue Dye over Novel Spherical Mesoporous $Cr_2O_3/TiO_2$ Nanoparticles Prepared by Sol-Gel Using Octadecylamine Template. *J. Environ. Chem. Eng.* **2017**, *5*, 4251–4261. [CrossRef]
156. Khasawneh, O.F.S.; Palaniandy, P.; Teng, L.P. Large-Scale Study for the Photocatalytic Degradation of Paracetamol Using $Fe_2O_3/TiO_2$ Nanocomposite Catalyst and CPC Reactor under Natural Sunlight Radiations. *MethodsX* **2019**, *6*, 2735–2743. [CrossRef]
157. Ortega-Liébana, M.C.; Sánchez-López, E.; Hidalgo-Carrillo, J.; Marinas, A.; Marinas, J.M.; Urbano, F.J. A Comparative Study of Photocatalytic Degradation of 3-Chloropyridine under UV and Solar Light by Homogeneous (Photo-Fenton) and Heterogeneous ($TiO_2$) Photocatalysis. *Appl. Catal. B Environ.* **2012**, *127*, 316–322. [CrossRef]
158. Stojilovic, N.; Scepanovic, M.; Grujic-Brojcin, M.; Golubovic, A.; Armakovic, S.; Abramovic, B.; Sreckovic, T.; Vasilic, R.; Dordevic, S.V.; Popovic, Z.V. Synthesis and Characterization of Titania-Based Nanopowders for Photocatalytic Degradation of Pindolol. *Bull. Am. Phys. Soc.* **2017**, *62*, 18.
159. Hazaraimi, M.H.; Goh, P.S.; Lau, W.J.; Ismail, A.F.; Wu, Z.; Subramaniam, M.N.; Lim, J.W.; Kanakaraju, D. The State-of-the-Art Development of Photocatalysts for Degrading of Persistent Herbicides in Aqueous Environment. *Sci. Total Environ.* **2022**, *843*, 156975. [CrossRef]
160. Islam, M.R.; Islam, J.B.; Furukawa, M.; Tateishi, I.; Katsumata, H.; Kaneco, S. Photocatalytic Degradation of a Systemic Herbicide: Picloram from Aqueous Solution Using Titanium Oxide ($TiO_2$) under Sunlight. *ChemEngineering* **2020**, *4*, 58. [CrossRef]
161. De Chiara, M.L.V.; Pal, S.; Licciulli, A.; Amodio, M.L.; Colelli, G. Photocatalytic Degradation of Ethylene on Mesoporous $TiO_2/SiO_2$ Nanocomposites: Effects on the Ripening of Mature Green Tomatoes. *Biosyst. Eng.* **2015**, *132*, 61–70. [CrossRef]
162. Paek, S.-M.; Jung, H.; Lee, Y.-J.; Park, M.; Hwang, S.-J.; Choy, J.-H. Exfoliation and Reassembling Route to Mesoporous Titania Nanohybrids. *Chem. Mater.* **2006**, *18*, 1134–1140. [CrossRef]
163. Alofi, S.; O'Rourke, C.; Mills, A. Photocatalytic Destruction of Stearic Acid by $TiO_2$ Films: Evidence of Highly Efficient Transport of Photogenerated Electrons and Holes. *J. Photochem. Photobiol. A Chem.* **2023**, *435*, 114273. [CrossRef]

164. Alofi, S.; O'Rourke, C.; Mills, A. Kinetics of Stearic Acid Destruction on $TiO_2$ 'Self-Cleaning'Films Revisited. *Photochem. Photobiol. Sci.* **2022**, *21*, 2061–2069. [CrossRef]
165. Smirnova, N.; Fesenko, T.; Zhukovsky, M.; Goworek, J.; Eremenko, A. Photodegradation of Stearic Acid Adsorbed on Superhydrophilic $TiO_2$ Surface: In Situ FT-IR and LDI Study. *Nanoscale Res. Lett.* **2015**, *10*, 500. [CrossRef]
166. Mills, A.; Lepre, A.; Elliott, N.; Bhopal, S.; Parkin, I.P.; O'neill, S.A. Characterisation of the Photocatalyst Pilkington Activ$^{TM}$: A Reference Film Photocatalyst? *J. Photochem. Photobiol. A Chem.* **2003**, *160*, 213–224. [CrossRef]
167. Matsunami, D.; Yamanaka, K.; Mizoguchi, T.; Kojima, K. Comparison of Photodegradation of Methylene Blue Using Various $TiO_2$ Films and $WO_3$ Powders under Ultraviolet and Visible-Light Irradiation. *J. Photochem. Photobiol. A Chem.* **2019**, *369*, 106–114. [CrossRef]
168. Zuo, R.; Du, G.; Zhang, W.; Liu, L.; Liu, Y.; Mei, L.; Li, Z. Photocatalytic Degradation of Methylene Blue Using $TiO_2$ Impregnated Diatomite. *Adv. Mater. Sci. Eng.* **2014**, *2014*, 170148. [CrossRef]
169. Hou, C.; Hu, B.; Zhu, J. Photocatalytic Degradation of Methylene Blue over $TiO_2$ Pretreated with Varying Concentrations of NaOH. *Catalysts* **2018**, *8*, 575. [CrossRef]
170. Kim, M.G.; Lee, J.E.; Kim, K.S.; Kang, J.M.; Lee, J.H.; Kim, K.H.; Cho, M.; Lee, S.G. Photocatalytic Degradation of Methylene Blue under UV and Visible Light by Brookite–Rutile Bi-Crystalline Phase of $TiO_2$. *New J. Chem.* **2021**, *45*, 3485–3497. [CrossRef]
171. Kader, S.; Al-Mamun, M.R.; Suhan, M.B.K.; Shuchi, S.B.; Islam, M.S. Enhanced Photodegradation of Methyl Orange Dye under UV Irradiation Using $MoO_3$ and Ag Doped $TiO_2$ Photocatalysts. *Environ. Technol. Innov.* **2022**, *27*, 102476. [CrossRef]
172. Wang, S.; Zhou, S. Photodegradation of Methyl Orange by Photocatalyst of CNTs/P-$TiO_2$ under UV and Visible-Light Irradiation. *J. Hazard. Mater.* **2011**, *185*, 77–85. [CrossRef] [PubMed]
173. Aziztyana, A.P.; Wardhani, S.; Prananto, Y.P.; Purwonugroho, D. Optimisation of Methyl Orange Photodegradation Using $TiO_2$-Zeolite Photocatalyst and $H_2O_2$ in Acid Condition. In Proceedings of the IOP Conference Series: Materials Science and Engineering; IOP Publishing: Bristol, UK, 2019; Volume 546, p. 42047.
174. Dong, H.; Zeng, G.; Tang, L.; Fan, C.; Zhang, C.; He, X.; He, Y. An Overview on Limitations of $TiO_2$-Based Particles for Photocatalytic Degradation of Organic Pollutants and the Corresponding Countermeasures. *Water Res.* **2015**, *79*, 128–146. [CrossRef]
175. Jin, C.; Liu, B.; Lei, Z.; Sun, J. Structure and Photoluminescence of the $TiO_2$ Films Grown by Atomic Layer Deposition Using Tetrakis-Dimethylamino Titanium and Ozone. *Nanoscale Res. Lett.* **2015**, *10*, 95. [CrossRef]
176. Leskelä, M.; Ritala, M. Atomic Layer Deposition (ALD): From Precursors to Thin Film Structures. *Thin Solid Films* **2002**, *409*, 138–146. [CrossRef]
177. Aarik, J.; Aidla, A.; Kiisler, A.-A.; Uustare, T.; Sammelselg, V. Effect of Crystal Structure on Optical Properties of $TiO_2$ Films Grown by Atomic Layer Deposition. *Thin Solid Films* **1997**, *305*, 270–273. [CrossRef]
178. Muñoz-Rojas, D.; Maindron, T.; Esteve, A.; Piallat, F.; Kools, J.C.S.; Decams, J.-M. Speeding up the Unique Assets of Atomic Layer Deposition. *Mater. Today Chem.* **2019**, *12*, 96–120. [CrossRef]
179. Jin, L.; Dai, B. $TiO_2$ Activation Using Acid-Treated Vermiculite as a Support: Characteristics and Photoreactivity. *Appl. Surf. Sci.* **2012**, *258*, 3386–3392. [CrossRef]
180. Sangiorgi, A.; Gonzalez, Z.; Ferrandez-Montero, A.; Yus, J.; Sanchez-Herencia, A.J.; Galassi, C.; Sanson, A.; Ferrari, B. 3D Printing of Photocatalytic Filters Using a Biopolymer to Immobilize $TiO_2$ Nanoparticles. *J. Electrochem. Soc.* **2019**, *166*, H3239–H3248. [CrossRef]
181. Luo, Y.; Cao, Y.; Guo, G. Effects of $TiO_2$ Nanoparticles on the Photodegradation of Poly (Lactic Acid). *J. Appl. Polym. Sci.* **2018**, *135*, 46509. [CrossRef]
182. Yang, L.; Liu, Z. Study on Light Intensity in the Process of Photocatalytic Degradation of Indoor Gaseous Formaldehyde for Saving Energy. *Energy Convers. Manag.* **2007**, *48*, 882–889. [CrossRef]
183. Ajmal, A.; Majeed, I.; Malik, R.N.; Idriss, H.; Nadeem, M.A. Principles and Mechanisms of Photocatalytic Dye Degradation on $TiO_2$ Based Photocatalysts: A Comparative Overview. *Rsc Adv.* **2014**, *4*, 37003–37026. [CrossRef]
184. Reza, K.M.; Kurny, A.S.W.; Gulshan, F. Parameters Affecting the Photocatalytic Degradation of Dyes Using $TiO_2$: A Review. *Appl. Water Sci.* **2017**, *7*, 1569–1578. [CrossRef]
185. Al-Nuaim, M.A.; Alwasiti, A.A.; Shnain, Z.Y. The Photocatalytic Process in the Treatment of Polluted Water. *Chem. Pap.* **2022**, 1–25. [CrossRef]
186. Pareek, V.; Chong, S.; Tadé, M.; Adesina, A.A. Light Intensity Distribution in Heterogenous Photocatalytic Reactors. *Asia Pacific J. Chem. Eng.* **2008**, *3*, 171–201. [CrossRef]
187. Herrmann, J.-M. Heterogeneous Photocatalysis: Fundamentals and Applications to the Removal of Various Types of Aqueous Pollutants. *Catal. Today* **1999**, *53*, 115–129. [CrossRef]
188. Kaneco, S.; Rahman, M.A.; Suzuki, T.; Katsumata, H.; Ohta, K. Optimization of Solar Photocatalytic Degradation Conditions of Bisphenol A in Water Using Titanium Dioxide. *J. Photochem. Photobiol. A Chem.* **2004**, *163*, 419–424. [CrossRef]
189. Kardar, P.; Ebrahimi, M.; Bastani, S. Influence of Temperature and Light Intensity on the Photocuring Process and Kinetics Parameters of a Pigmented UV Curable System. *J. Therm. Anal. Calorim.* **2014**, *118*, 541–549. [CrossRef]
190. Rusu, M.C.; Block, C.; Van Assche, G.; Van Mele, B. Influence of Temperature and UV Intensity on Photo-Polymerization Reaction Studied by Photo-DSC. *J. Therm. Anal. Calorim.* **2012**, *110*, 287–294. [CrossRef]

191. He, H.; Li, L.; Lee, L.J. Photopolymerization and Structure Formation of Methacrylic Acid Based Hydrogels: The Effect of Light Intensity. *React. Funct. Polym.* **2008**, *68*, 103–113. [CrossRef]
192. Terrones, G.; Pearlstein, A.J. Effects of Kinetics and Optical Attenuation on the Completeness, Uniformity, and Dynamics of Monomer Conversion in Free-Radical Photopolymerizations. *Macromolecules* **2001**, *34*, 8894–8906. [CrossRef]
193. Doğruyol, Z.; Arsu, N.; Pekcan, Ö. Critical Exponents of Photoinitiated Gelation at Different Light Intensities. *J. Macromol. Sci. Part B* **2009**, *48*, 745–754. [CrossRef]
194. Thiher, N.L.K.; Schissel, S.M.; Jessop, J.L.P. Quantifying UV/EB Dual Cure for Successful Mitigation of Oxygen Inhibition and Light Attenuation. *Prog. Org. Coat.* **2020**, *138*, 105378. [CrossRef]
195. Alsheheri, S.Z. Nanocomposites Containing Titanium Dioxide for Environmental Remediation. *Des. Monomers Polym.* **2021**, *24*, 22–45. [CrossRef]
196. Zhu, H.; Jiang, R.; Fu, Y.; Guan, Y.; Yao, J.; Xiao, L.; Zeng, G. Effective Photocatalytic Decolorization of Methyl Orange Utilizing $TiO_2$/ZnO/Chitosan Nanocomposite Films under Simulated Solar Irradiation. *Desalination* **2012**, *286*, 41–48. [CrossRef]
197. Takahatake, Y.; Shibata, A.; Nomura, K.; Sato, T. Effect of Flowing Water on Sr Sorption Changes of Hydrous Sodium Titanate. *Minerals* **2017**, *7*, 247. [CrossRef]
198. Bahrudin, N.N. Evaluation of Degradation Kinetic and Photostability of Immobilized $TiO_2$/Activated Carbon Bilayer Photocatalyst for Phenol Removal. *Appl. Surf. Sci. Adv.* **2022**, *7*, 100208. [CrossRef]
199. Hapeshi, E.; Achilleos, A.; Vasquez, M.I.; Michael, C.; Xekoukoulotakis, N.P.; Mantzavinos, D.; Kassinos, D. Drugs Degrading Photocatalytically: Kinetics and Mechanisms of Ofloxacin and Atenolol Removal on Titania Suspensions. *Water Res.* **2010**, *44*, 1737–1746. [CrossRef]
200. Maeng, S.K.; Cho, K.; Jeong, B.; Lee, J.; Lee, Y.; Lee, C.; Choi, K.J.; Hong, S.W. Substrate-Immobilized Electrospun $TiO_2$ Nanofibers for Photocatalytic Degradation of Pharmaceuticals: The Effects of PH and Dissolved Organic Matter Characteristics. *Water Res.* **2015**, *86*, 25–34. [CrossRef]
201. Fawzy, A.; Mahanna, H.; Mossad, M. Effective Photocatalytic Degradation of Amoxicillin Using MIL-53 (Al)/ZnO Composite. *Environ. Sci. Pollut. Res.* **2022**, *29*, 68532–68546. [CrossRef]
202. Alam, U.; Khan, A.; Raza, W.; Khan, A.; Bahnemann, D.; Muneer, M. Highly Efficient Y and V Co-Doped ZnO Photocatalyst with Enhanced Dye Sensitized Visible Light Photocatalytic Activity. *Catal. Today* **2017**, *284*, 169–178. [CrossRef]
203. Kalaivani, T.; Anilkumar, P. Role of Temperature on the Phase Modification of $TiO_2$ Nanoparticles Synthesized by the Precipitation Method. *Silicon* **2018**, *10*, 1679–1686. [CrossRef]
204. Henderson, M.A. A Surface Science Perspective on $TiO_2$ Photocatalysis. *Surf. Sci. Rep.* **2011**, *66*, 185–297. [CrossRef]
205. Jamil, S.; Fasehullah, M. Effect of Temperature on Structure, Morphology, and Optical Properties of $TiO_2$ Nanoparticles. *Mater. Innovations* **2021**, *1*, 22–28. [CrossRef]
206. Panagiotopoulou, P.; Kondarides, D.I. Effect of Morphological Characteristics of $TiO_2$-Supported Noble Metal Catalysts on Their Activity for the Water–Gas Shift Reaction. *J. Catal.* **2004**, *225*, 327–336. [CrossRef]
207. Yu, K.; Zhao, J.; Guo, Y.; Ding, X.; Liu, Y.; Wang, Z. Sol–Gel Synthesis and Hydrothermal Processing of Anatase Nanocrystals from Titanium n-Butoxide. *Mater. Lett.* **2005**, *59*, 2515–2518. [CrossRef]
208. Elsellami, L.; Dappozze, F.; Fessi, N.; Houas, A.; Guillard, C. Highly Photocatalytic Activity of Nanocrystalline $TiO_2$ (Anatase, Rutile) Powders Prepared from TiCl4 by Sol–Gel Method in Aqueous Solutions. *Process Saf. Environ. Prot.* **2018**, *113*, 109–121. [CrossRef]
209. Chen, Y.-F.; Lee, C.-Y.; Yeng, M.-Y.; Chiu, H.-T. The Effect of Calcination Temperature on the Crystallinity of $TiO_2$ Nanopowders. *J. Cryst. Growth* **2003**, *247*, 363–370. [CrossRef]
210. Bessekhouad, Y.; Robert, D.; Weber, J. V Preparation of $TiO_2$ Nanoparticles by Sol-Gel Route. *Int. J. Photoenergy* **2003**, *5*, 153–158. [CrossRef]
211. Velardi, L.; Scrimieri, L.; Serra, A.; Manno, D.; Calcagnile, L. Effect of Temperature on the Physical, Optical and Photocatalytic Properties of $TiO_2$ Nanoparticles. *SN Appl. Sci.* **2020**, *2*, 707. [CrossRef]
212. Nezar, S.; Laoufi, N.A. Electron Acceptors Effect on Photocatalytic Degradation of Metformin under Sunlight Irradiation. *Sol. Energy* **2018**, *164*, 267–275. [CrossRef]
213. Mao, S.; Bao, R.; Fang, D.; Yi, J. Influence of Electron Acceptor and Carrier in Amorphous $TiO_2$ upon the Photocatalytic Degradation of Methylene Orange. *Mater. Res. Express* **2018**, *5*, 45051. [CrossRef]
214. Ahmed, S.; Rasul, M.G.; Brown, R.; Hashib, M.A. Influence of Parameters on the Heterogeneous Photocatalytic Degradation of Pesticides and Phenolic Contaminants in Wastewater: A Short Review. *J. Environ. Manag.* **2011**, *92*, 311–330. [CrossRef] [PubMed]
215. Grushevskaya, S.; Belyanskaya, I.; Kozaderov, O. Approaches for Modifying Oxide-Semiconductor Materials to Increase the Efficiency of Photocatalytic Water Splitting. *Materials* **2022**, *15*, 4915. [CrossRef]
216. Pesci, F.M.; Wang, G.; Klug, D.R.; Li, Y.; Cowan, A.J. Efficient Suppression of Electron–Hole Recombination in Oxygen-Deficient Hydrogen-Treated $TiO_2$ Nanowires for Photoelectrochemical Water Splitting. *J. Phys. Chem. C* **2013**, *117*, 25837–25844. [CrossRef]
217. Ulusoy, T.G. Development of Photoanodes for Performance Enhanced Dye Sensitized Solar Cells. Doctoral Dissertation, Bilkent Universitesi, Çankaya, Turkey, 2015.
218. Kashif, N.; Ouyang, F. Parameters Effect on Heterogeneous Photocatalysed Degradation of Phenol in Aqueous Dispersion of $TiO_2$. *J. Environ. Sci.* **2009**, *21*, 527–533. [CrossRef]

219. Pizzino, G.; Irrera, N.; Cucinotta, M.; Pallio, G.; Mannino, F.; Arcoraci, V.; Squadrito, F.; Altavilla, D.; Bitto, A. Oxidative Stress: Harms and Benefits for Human Health. *Oxid. Med. Cell. Longev.* **2017**, *2017*, 8416763. [CrossRef]
220. Vučić, M.D.R.; Mitrović, J.Z.; Kostić, M.M.; Velinov, N.D.; Najdanović, S.M.; Bojić, D.V. Heterogeneous Photocatalytic Degradation of Anthraquinone Dye Reactive Blue 19: Optimization, Comparison between Processes and Identification of Intermediate Products. *Water Sa* **2020**, *46*, 291–299.
221. Saquib, M.; Muneer, M. Photocatalytic Degradation of Two Selected Textile Dye Derivatives, Eosine Yellowish and p-Rosaniline, in Aqueous Suspensions of Titanium Dioxide. *J. Environ. Sci. Heal. Part A* **2003**, *38*, 2581–2598. [CrossRef]
222. Liu, Q.T.; Williams, T.D.; Cumming, R.I.; Holm, G.; Hetheridge, M.J.; Murray-Smith, R. Comparative Aquatic Toxicity of Propranolol and Its Photodegraded Mixtures: Algae and Rotifer Screening. *Environ. Toxicol. Chem.* **2009**, *28*, 2622–2631. [CrossRef]
223. Zebardast, M.; Fallah Shojaei, A.; Tabatabaeian, K. Enhanced Removal of Methylene Blue Dye by Bimetallic Nano-Sized MOF-5s. *Iran. J. Catal.* **2018**, *8*, 297–309.
224. Sharma, P.; Slater, T.J.A.; Sharma, M.; Bowker, M.; Catlow, C.R.A. Enhanced $H_2O_2$ Production via Photocatalytic $O_2$ Reduction over Structurally-Modified Poly (Heptazine Imide). *Chem. Mater.* **2022**, *34*, 5511–5521. [CrossRef]
225. Mir, N.A.; Haque, M.M.; Khan, A.; Muneer, M.; Boxall, C. Photoassisted Degradation of a Herbicide Derivative, Dinoseb, in Aqueous Suspension of Titania. *Sci. World J.* **2012**, *2012*, 251527. [CrossRef]
226. Mir, N.A.; Khan, A.; Dar, A.A.; Muneer, M. Photocatalytic Study of Two Azo Dye Derivatives, Ponceau Bs and Reactive Blue 160 in Aqueous Suspension of $TiO_2$: Adsorption Isotherm and Decolorization Kinetics. *IJIRSET* **2014**, *3*, 933–9348.
227. Yang, Y.; Cheng, B.; Yu, J.; Wang, L.; Ho, W. $TiO_2/In_2S_3$ S-Scheme Photocatalyst with Enhanced $H_2O_2$-Production Activity. *Nano Res.* **2021**, 1–9. [CrossRef]
228. Muruganandham, M.; Swaminathan, M. Photocatalytic Decolourisation and Degradation of Reactive Orange 4 by $TiO_2$-UV Process. *Dye. Pigment.* **2006**, *68*, 133–142. [CrossRef]
229. Liu, X.; Zhang, T.; Shao, Y. Aqueous Bromate Reduction by UV Activation of Sulfite. *CLEAN Soil Air Water* **2014**, *42*, 1370–1375. [CrossRef]
230. Poulios, I.; Kositzi, M.; Kouras, A. Photocatalytic Decomposition of Triclopyr over Aqueous Semiconductor Suspensions. *J. Photochem. Photobiol. A Chem.* **1998**, *115*, 175–183. [CrossRef]
231. Pędziwiatr, P. Decomposition of Hydrogen Peroxide-Kinetics and Review of Chosen Catalysts. *Acta Innov.* **2018**, *26*, 45–52. [CrossRef]
232. Zhang, W.; Sun, W.; Zhang, Y.; Yu, D.; Piao, W.; Wei, H.; Liu, X.; Sun, C. Effect of Inorganic Salt on the Removal of Typical Pollutants in Wastewater by $RuO_2/TiO_2$ via Catalytic Wet Air Oxidation. *Chemosphere* **2022**, *312*, 137194. [CrossRef] [PubMed]
233. Ma, J.; Yang, Y.; Jiang, X.; Xie, Z.; Li, X.; Chen, C.; Chen, H. Impacts of Inorganic Anions and Natural Organic Matter on Thermally Activated Persulfate Oxidation of BTEX in Water. *Chemosphere* **2018**, *190*, 296–306. [CrossRef]
234. Sánchez-Polo, M.; Ocampo-Pérez, R.; Rivera-Utrilla, J.; Mota, A.J. Comparative Study of the Photodegradation of Bisphenol A by HO, $SO_4-$ and $CO_3-/HCO_3$ Radicals in Aqueous Phase. *Sci. Total Environ.* **2013**, *463*, 423–431. [CrossRef] [PubMed]
235. Liao, C.-H.; Kang, S.-F.; Wu, F.-A. Hydroxyl Radical Scavenging Role of Chloride and Bicarbonate Ions in the $H_2O_2$/UV Process. *Chemosphere* **2001**, *44*, 1193–1200. [CrossRef] [PubMed]
236. Lutze, H.V.; Kerlin, N.; Schmidt, T.C. Sulfate Radical-Based Water Treatment in Presence of Chloride: Formation of Chlorate, Inter-Conversion of Sulfate Radicals into Hydroxyl Radicals and Influence of Bicarbonate. *Water Res.* **2015**, *72*, 349–360. [CrossRef]
237. Al-Mamary, M.A.; Moussa, Z. Antioxidant Activity: The Presence and Impact of Hydroxyl Groups in Small Molecules of Natural and Synthetic Origin. In *Antioxidants—Benefits, Sources, Mechanisms of Action*; IntechOpen: London, UK, 2021; pp. 318–377.
238. Lu, C.-S.; Chen, C.-C.; Mai, F.-D.; Li, H.-K. Identification of the Degradation Pathways of Alkanolamines with $TiO_2$ Photocatalysis. *J. Hazard. Mater.* **2009**, *165*, 306–316. [CrossRef]
239. Wang, Z.; Yuan, R.; Guo, Y.; Xu, L.; Liu, J. Effects of Chloride Ions on Bleaching of Azo Dyes by $Co^{2+}$/Oxone Regent: Kinetic Analysis. *J. Hazard. Mater.* **2011**, *190*, 1083–1087. [CrossRef]
240. Zhu, H.; Jiang, R.; Xiao, L.; Chang, Y.; Guan, Y.; Li, X.; Zeng, G. Photocatalytic Decolorization and Degradation of Congo Red on Innovative Crosslinked Chitosan/Nano-CdS Composite Catalyst under Visible Light Irradiation. *J. Hazard. Mater.* **2009**, *169*, 933–940. [CrossRef]
241. Pandi, K.; Preeyanghaa, M.; Vinesh, V.; Madhavan, J.; Neppolian, B. Complete Photocatalytic Degradation of Tetracycline by Carbon Doped $TiO_2$ Supported with Stable Metal Nitrate Hydroxide. *Environ. Res.* **2022**, *207*, 112188. [CrossRef]
242. Mertah, O.; Gómez-Avilés, A.; Kherbeche, A.; Belver, C.; Bedia, J. Peroxymonosulfate Enhanced Photodegradation of Sulfamethoxazole with $TiO_2$@ $CuCo_2O_4$ Catalysts under Simulated Solar Light. *J. Environ. Chem. Eng.* **2022**, *10*, 108438. [CrossRef]
243. Riga, A.; Soutsas, K.; Ntampegliotis, K.; Karayannis, V.; Papapolymerou, G. Effect of System Parameters and of Inorganic Salts on the Decolorization and Degradation of Procion H-Exl Dyes. Comparison of $H_2O_2$/UV, Fenton, UV/Fenton, $TiO_2$/UV and $TiO_2/UV/H_2O_2$ Processes. *Desalination* **2007**, *211*, 72–86. [CrossRef]
244. Mahvi, A.H.; Ghanbarian, M.; Nasseri, S.; Khairi, A. Mineralization and Discoloration of Textile Wastewater by $TiO_2$ Nanoparticles. *Desalination* **2009**, *239*, 309–316. [CrossRef]
245. Ganiyu, S.O.; El-Din, M.G. Insight into In-Situ Radical and Non-Radical Oxidative Degradation of Organic Compounds in Complex Real Matrix during Electrooxidation with Boron Doped Diamond Electrode: A Case Study of Oil Sands Process Water Treatment. *Appl. Catal. B Environ.* **2020**, *279*, 119366. [CrossRef]

246. Wang, R.; Hashimoto, K.; Fujishima, A.; Chikuni, M.; Kojima, E.; Kitamura, A.; Shimohigoshi, M.; Watanabe, T. Light-Induced Amphiphilic Surfaces. *Nature* **1997**, *388*, 431–432. [CrossRef]
247. Zhang, M.; Lei, E.; Zhang, R.; Liu, Z. The Effect of $SiO_2$ on $TiO_2$-$SiO_2$ Composite Film for Self-Cleaning Application. *Surf. Interfaces* **2019**, *16*, 194–198. [CrossRef]
248. Kawasaki, S.; Holmström, E.; Takahashi, R.; Spijker, P.; Foster, A.S.; Onishi, H.; Lippmaa, M. Intrinsic Superhydrophilicity of Titania-Terminated Surfaces. *J. Phys. Chem. C* **2017**, *121*, 2268–2275. [CrossRef]
249. Sakai, N.; Fujishima, A.; Watanabe, T.; Hashimoto, K. Quantitative Evaluation of the Photoinduced Hydrophilic Conversion Properties of $TiO_2$ Thin Film Surfaces by the Reciprocal of Contact Angle. *J. Phys. Chem. B* **2003**, *107*, 1028–1035. [CrossRef]
250. Mao, C.; Wang, X.; Zhang, W.; Hu, B.; Deng, H. Super-Hydrophilic $TiO_2$-Based Coating of Anion Exchange Membranes with Improved Antifouling Performance. *Colloids Surf. A Physicochem. Eng. Asp.* **2021**, *614*, 126136. [CrossRef]
251. Siebenhofer, M.; Viernstein, A.; Morgenbesser, M.; Fleig, J.; Kubicek, M. Photoinduced Electronic and Ionic Effects in Strontium Titanate. *Mater. Adv.* **2021**, *2*, 7583–7619. [CrossRef]
252. Kim, H.-M.; Kim, D.; Kim, B. Photoinduced Hydrophilicity of $TiO_2/WO_3$ Double Layer Films. *Surf. Coatings Technol.* **2015**, *271*, 18–21. [CrossRef]
253. Banerjee, S.; Dionysiou, D.D.; Pillai, S.C. Self-Cleaning Applications of $TiO_2$ by Photo-Induced Hydrophilicity and Photocatalysis. *Appl. Catal. B Environ.* **2015**, *176*, 396–428. [CrossRef]
254. De Jesus, M.A.M.L.; da Neto, J.T.S.; Timò, G.; Paiva, P.R.P.; Dantas, M.S.S.; de Ferreira, A.M. Superhydrophilic Self-Cleaning Surfaces Based on $TiO_2$ and $TiO_2/SiO_2$ Composite Films for Photovoltaic Module Cover Glass. *Appl. Adhes. Sci.* **2015**, *3*, 5. [CrossRef]
255. Chen, H.; Li, X.; Li, D. Superhydrophilic–Superhydrophobic Patterned Surfaces: From Simplified Fabrication to Emerging Applications. *Nanotechnol. Precis. Eng.* **2022**, *5*, 35002. [CrossRef]
256. Okkay, H.; Satı, S.; Cengiz, U. Mechanically Stable Superhydrophilic Antifog Surface by Microwave Assisted Sol-Gel Method. *J. Taiwan Inst. Chem. Eng.* **2021**, *120*, 360–367. [CrossRef]
257. Adachi, T.; Latthe, S.S.; Gosavi, S.W.; Roy, N.; Suzuki, N.; Ikari, H.; Kato, K.; Katsumata, K.; Nakata, K.; Furudate, M. Photocatalytic, Superhydrophilic, Self-Cleaning $TiO_2$ Coating on Cheap, Light-Weight, Flexible Polycarbonate Substrates. *Appl. Surf. Sci.* **2018**, *458*, 917–923. [CrossRef]
258. Kameya, Y.; Yabe, H. Optical and Superhydrophilic Characteristics of $TiO_2$ Coating with Subwavelength Surface Structure Consisting of Spherical Nanoparticle Aggregates. *Coatings* **2019**, *9*, 547. [CrossRef]
259. Pellegrino, F.; Pellutiè, L.; Sordello, F.; Minero, C.; Ortel, E.; Hodoroaba, V.-D.; Maurino, V. Influence of Agglomeration and Aggregation on the Photocatalytic Activity of $TiO_2$ Nanoparticles. *Appl. Catal. B Environ.* **2017**, *216*, 80–87. [CrossRef]
260. Wang, C.; Böttcher, C.; Bahnemann, D.W.; Dohrmann, J.K. A Comparative Study of Nanometer Sized Fe (III)-Doped $TiO_2$ Photocatalysts: Synthesis, Characterization and Activity. *J. Mater. Chem.* **2003**, *13*, 2322–2329. [CrossRef]
261. Zhang, H.; Wang, D.; Han, Y.; Tang, Q.; Wu, H.; Mao, N. High Photoactivity Rutile-Type $TiO_2$ Particles Co-Doped with Multiple Elements under Visible Light Irradiation. *Mater. Res. Express* **2018**, *5*, 105015. [CrossRef]
262. Tolosana-Moranchel, A.; Pecharromán, C.; Faraldos, M.; Bahamonde, A. Strong Effect of Light Scattering by Distribution of $TiO_2$ Particle Aggregates on Photocatalytic Efficiency in Aqueous Suspensions. *Chem. Eng. J.* **2021**, *403*, 126186. [CrossRef]
263. Liu, Y.; Tang, A.; Zhang, Q.; Yin, Y. Seed-Mediated Growth of Anatase $TiO_2$ Nanocrystals with Core–Antenna Structures for Enhanced Photocatalytic Activity. *J. Am. Chem. Soc.* **2015**, *137*, 11327–11339. [CrossRef]
264. Yang, Y.; Li, J.; Zhang, H.; Wang, G.; Rao, Y.; Gan, G. $TiO_2$ Tailored Low Loss NiCuZn Ferrite Ceramics Having Equivalent Permeability and Permittivity for Miniaturized Antenna. *J. Magn. Magn. Mater.* **2019**, *487*, 165318. [CrossRef]
265. Han, C.; Gómez, D.E.; Xiao, Q.; Xu, J. Near-Field Enhancement by Plasmonic Antennas for Photocatalytic Suzuki-Miyaura Cross-Coupling Reactions. *J. Catal.* **2021**, *397*, 205–211. [CrossRef]
266. Gao, S.; Ueno, K.; Misawa, H. Plasmonic Antenna Effects on Photochemical Reactions. *Acc. Chem. Res.* **2011**, *44*, 251–260. [CrossRef]
267. Han, P.; Tana, T.; Xiao, Q.; Sarina, S.; Waclawik, E.R.; Gómez, D.E.; Zhu, H. Promoting Ni (II) Catalysis with Plasmonic Antennas. *Chem* **2019**, *5*, 2879–2899. [CrossRef]
268. Gellé, A.; Price, G.D.; Voisard, F.; Brodusch, N.; Gauvin, R.; Amara, Z.; Moores, A. Enhancing Singlet Oxygen Photocatalysis with Plasmonic Nanoparticles. *ACS Appl. Mater. Interfaces* **2021**, *13*, 35606–35616. [CrossRef]
269. Lei, S.H.I.; Duan, W. Highly Active Mixed-Phase $TiO_2$ Photocatalysts Fabricated at Low Temperatureand the Correlation between Phase Compositionand Photocatalytic Activity. *J. Environ. Sci.* **2008**, *20*, 1263–1267.
270. Porcu, S.; Secci, F.; Ricci, P.C. Advances in Hybrid Composites for Photocatalytic Applications: A Review. *Molecules* **2022**, *27*, 6828. [CrossRef]
271. Faccani, L.; Ortelli, S.; Blosi, M.; Costa, A.L. Ceramized Fabrics and Their Integration in a Semi-Pilot Plant for the Photodegradation of Water Pollutants. *Catalysts* **2021**, *11*, 1418. [CrossRef]

272. Malato, S.; Maldonado, M.I.; Fernandez-Ibanez, P.; Oller, I.; Polo, I.; Sánchez-Moreno, R. Decontamination and Disinfection of Water by Solar Photocatalysis: The Pilot Plants of the Plataforma Solar de Almeria. *Mater. Sci. Semicond. Process.* **2016**, *42*, 15–23. [CrossRef]
273. Fendrich, M.A.; Quaranta, A.; Orlandi, M.; Bettonte, M.; Miotello, A. Solar Concentration for Wastewaters Remediation: A Review of Materials and Technologies. *Appl. Sci.* **2018**, *9*, 118. [CrossRef]